Chemical Geology 391 (2015) 19–32

Contents lists available at ScienceDirect

Chemical Geology

journal homepage: www.elsevier.com/locate/chemgeo

Rare earth elements as reactive tracers of biogeochemical weathering in forested rhyolitic terrain

Angélica Vázquez-Ortega [a], Julia Perdrial [a], Adrian Harpold [b,d], Xavier Zapata-Ríos [b], Craig Rasmussen [a], Jennifer McIntosh [b], Marcel Schaap [a], Jon D. Pelletier [c], Paul D. Brooks [b], Mary Kay Amistadi [a], Jon Chorover [a,c,*]

[a] Department of Soil, Water & Environmental Science, University of Arizona, 1177 East Fourth Street, Tucson, AZ 85721-0038, USA
[b] Department of Hydrology and Water Resources, University of Arizona, 1133 East James E. Rogers Way, Tucson, AZ 85721-0011, USA
[c] Department of Geosciences, University of Arizona, 1040 East Fourth Street, Tucson, AZ 85721-0077, USA
[d] Institute of Arctic and Alpine Research, University of Colorado, 1560 30th Street, Boulder, CO 80303-0450, USA

ARTICLE INFO

Article history:
Received 7 April 2014
Received in revised form 16 October 2014
Accepted 17 October 2014
Available online 29 October 2014

Editor: J. Fein

Keywords:
Rare earth elements
Dissolved organic carbon
Ce-anomaly
Eu-anomaly
Biological weathering
Critical zone

ABSTRACT

Rare earth elements (REEs) were evaluated as potential tracers of biogeochemical weathering at pedon, hillslope, and catchment scales in the Jemez River Basin Critical Zone Observatory (JRB-CZO), Valles Caldera National Preserve, NM, USA. We investigated time series of REE patterns in precipitation, soil pore water, groundwater, and stream water, and related these data to REE composition of soil, rock and atmospheric dust. REE signatures in stream waters are dynamic, reflecting processes that occur along hydrologic flowpaths during transport to the stream, including organic matter complexation, primary and secondary mineral weathering, water/soil/bedrock interaction, and atmospheric deposition. Strong compositional similarities for the REE between soil waters and stream waters during the initial snowmelt are consistent with shallow subsurface flows to streams. Most (bio) chemical denudation of REE occurred during the snowmelt-derived dissolved organic carbon (DOC) pulse, during which time apparent colloidal mobilization of REE occurred in association with Fe and Al (oxy)hydroxides. The REE and DOC concentrations in stream waters were positively correlated ($R^2 = 0.80$, $p < 0.0001$) during snowmelt, suggesting REE complexation and mobilization in association with organic ligands during the period of shallow subsurface flow. Positive Eu-anomalies occur in the soil matrix ($[Eu / Eu^*]_{RT}$ range from 1.79 to 2.52), soil solutions ($[Eu / Eu^*]_{RT}$ range from 1.89 to 5.98), and stream waters ($[Eu / Eu^*]_{RT}$ range from 1.01 to 2.27) with respect to the host lithologies—effects attributable to both eolian deposition and preferential feldspar dissolution. Cerium anomalies in soil solids and porewaters indicate seasonally dynamic translocation and oxidative accumulation in subsurface soil horizons (surface horizons: $[Ce / Ce^*]_{RT}$ range from 0.70 to 1.1; subsurface horizons: $[Ce / Ce^*]_{RT}$ range from 0.95 to 1.29), consistent with prior research reporting Ce(IV) co-precipitation with Fe- and Mn-oxide minerals.

1. Introduction

Prior studies have shown the potential for lanthanide series metals (i.e., "rare earth elements" or REE) to serve as reactive tracers of biogeochemical processes in low temperature systems (e.g., Elderfield et al., 1990; Johannesson et al., 1997, 2004, 2014; Leybourne and Johannesson, 2008; Shiller, 2010; Tang and Johannesson, 2010b; Willis and Johannesson, 2011; Gangloff et al., 2014; Guo et al., 2010; Steinmann and Stille, 2006, 2008; Stille et al., 2006). The unique chemical properties of trivalent Lewis acid REE include a systematic increase in ionic potential (valence normalized to ionic radius) with increasing atomic number (Z). Systematic variation in metal-ligand chemical reactivity makes the REE useful for studying biological impacts on weathering in the earth's critical zone (NRC, 2001) because of the documented variation in their tendency to form stable complexes with organic and inorganic ligands common to natural waters (Wood, 1990; Byrne and Li, 1995; Davranche et al., 2004, 2005; Sonke and Salters, 2006; Pourret et al., 2007a,b; Pourret and Martinez, 2009; Yamamoto et al., 2010; Grybos et al., 2007). Hence their mobilization (i.e., chemical denudation) from a bioactive weathering profile and into stream drainage waters may be strongly influenced by incongruent weathering reactions and organic carbon flux (Dupre et al., 1999; Gruau et al., 2004; Pourret et al., 2010).

Aqueous geochemical signatures of streams vary with time because of dynamic mixing of waters from spatially distinct catchment locations (Nakajima and Terakado, 2003; Bailey et al., 2004; Voegelin et al., 2012) including biological "hot-spots" (McClain et al., 2003). Therefore, occurrences of REE-enriched discharge, and REE fractionation patterns may help to constrain the timing and spatial distribution of weathering in upland soils and to help resolve the temporal dynamics of catchment bio-

* Corresponding author at: Department of Soil, Water & Environmental Science, University of Arizona, 1177 East Fourth Street, Tucson, Arizona 85721-0038, USA.
E-mail address: chorover@email.arizona.edu (J. Chorover).

http://dx.doi.org/10.1016/j.chemgeo.2014.10.016
0009-2541/

weathering in particular (Dupre et al., 1999; Pourret et al., 2007a,b, 2010). To the extent that different critical zone water sources might be shown to produce distinct rare earth element and yttrium (REY) signatures and/or concentrations, as well as dynamic changes in the same over hydrologic events, we postulated that they may also be useful to resolving up-gradient biological weathering processes in natural catchments.

Variation in REY fractionation patterns during chemical denudation reflects their relative mobilities, in turn controlled by the formation of mobile aqueous complexes (organic and inorganic), as well as sorption and co-precipitation effects (Sonke and Salters, 2006; Pourret et al., 2007a; Laveuf and Cornu, 2009; Goyne et al., 2010). However, the impacts of DOM complexation on REY release during regolith weathering remain unclear. For example, DOM has been shown to be preferentially enriched in heavy REEs (HREE: Dy to Lu) because of their smaller ionic radii (the "lanthanide contraction effect") favoring incorporation into stable complexes with acidic organic functional groups (Sonke and Salters, 2006). Conversely, Davranche et al. (2011) reported middle (M)REE downward concavity patterns in soil solutions during wetland soil reduction, attributing to DOM a tendency to concentrate MREE. In either case, REY-ligand complexation affects non-stoichiometric dissolution of primary minerals (Goyne et al., 2010) and the effective solubilization and transport of complexed REY in natural waters (Xiong, 2011).

Because of their +3 charge, REEs are subject to adsorption at surfaces of secondary minerals (Bau, 1999; Bau and Koschinsky, 2009), and scavenging by Fe, Mn, and Al-(oxy)hydroxides during co-precipitation (Bau, 1999; Ohta and Kawabe, 2001). As a result of their high affinity for Mn-, Fe-(oxyhydr)oxides, REEs are postulated to also cycle in and out of soil pore waters during dissolution-precipitation via redox or non-redox derived mechanisms (Pokrovsky and Schott, 2002; Davranche et al., 2011), especially as pore waters fluctuate between supersaturated and undersaturated conditions with respect to REE-sorbing solid phases (Thompson et al., 2006b). In addition to dissolution-induced REE release, high specific surface area colloidal organo-mineral complexes are also mobilized during precipitation (e.g. rainfall) events. Pulsed colloidal (<1 μm particulate) dispersion or coagulation may result from wetting–drying events that promote excursions in pH or redox status driven by rapid microbial response. Prior experimental studies indicate that fluctuations in Eh/pH of natural soils induce colloidal dispersion that mobilizes nano-particles enriched in the lanthanide series metals (Viers et al., 1997; Braun et al., 1998; Thompson et al., 2006a, 2013). Redox conditions therefore likely influence REE fractionation through these multiple indirect mechanisms in soils and aquatic environments (Elderfield, 1988; Moffett, 1994; Bau and Koschinsky, 2009; Davranche et al., 2011).

Redox effects on REE fractionation can be direct as well, however, as europium and cerium are both redox sensitive. Eu deviates from the other REE in that it occurs in both (III) and (II) valence states. Reduction of Eu(III) requires strong reducing conditions rarely encountered in low pressure-temperature systems (Panahi et al., 2000; Laveuf and Cornu, 2009), but Eu(II) predominates in magmatic systems (Henderson, 1996), and bivalent Eu is introduced to the critical zone in primary tectosilicate minerals such as feldspars (K-feldspar and plagioclases), where it substitutes preferentially into Ca^{2+}, Na^{+}, and K^{+} sites (Schnetzl and Philpott, 1970). Preferential dissolution of feldspars relative to other REE-bearing primary minerals should, therefore, result in positive aqueous Eu-anomalies (Ma et al., 2011; Brioschi et al., 2013).

Conversely, Ce occurs in (III) or (IV) valence states in soils and sediments. The oxidation of Ce(III) occurs at Eh values around 300 mV (De Carlo and Wen, 1998), a condition that is commonly encountered in sub-oxic to oxic surficial environments. This induces changes in ionic charge and radius that decouple Ce(IV) from the rest of the REE, commonly promoting its secondary solid phase incorporation, generating positive Ce anomalies in soils (Feng, 2010; Laveuf et al., 2012).

Given that radius- and redox-state-dependent fractionation of REY occur in low temperature geochemical systems, the current work sought to assess whether REY trends in rock, soil and natural water could be applied to resolve aspects of biogeochemical weathering resulting from snowmelt events in seasonally-snow covered nested catchments located in the JRB-CZO. The principal objectives were (i) to explore whether REY patterns of critical zone catchment sources are reflected in time dynamics of stream water REY efflux, including their changes with time and spatial scale and (ii) to reveal biogeochemical processes influencing catchment REY fractionation during snowmelt events. We postulated that pore and stream waters of the snowmelt period would contain useful REY signatures of biological weathering from the upland source areas.

2. Materials and methods

2.1. Study site

The field experimental design takes advantage of a nested headwater catchment infrastructure located in montane mixed conifer forests within the Jemez River Basin Critical Zone Observatory (JRB-CZO) (Brooks and Vivoni, 2008; Chorover et al., 2011) in the Valles Caldera National Preserve, northern New Mexico (Fig. 1A). The JRB-CZO is instrumented to monitor CZ processes including fluid (gas, water and solute) flows from pedon to catchment scales (Fig. 1, also see http://criticalzone.org/catalina-jemez/). Instrumented pedon sites were located within a zero order basin (ZOB) (Fig. 1D) on Redondo Dome (35°52′56″N, 106°32′8″W) within the larger La Jara catchment (LJC, Fig. 1C). The ZOB is south-oriented with dominant SW and SE facing slopes like most of the larger East Fork Jemez watershed (EFJW, Fig. 1B). Most of Redondo Dome, including the ZOB, is underlain by Pleistocene aged rhyolitic volcaniclastics of the Tewa Group (http://geoinfo.nmt.edu/publications/maps/geologic/ofgm/). The bedrock within the ZOB is comprised of a combination of dense, highly fractured porphyritic rhyodacite that underlies 45–50% of the ZOB, and partially welded and hydrothermally altered Bandelier Tuff that occupies the other 50–55%. The rhyodacite mineral composition includes 25–30% quartz, 40–45% plagioclase feldspar (albite and oligoclase), and 25–30% alkali feldspar (sanidine) with a density near 2.6 g/cm^3, whereas the Bandelier Tuff composition can be more variable depending on degree of hydrothermal alteration. The tuff sampled from the ZOB exhibited a mineral composition of (on a mass basis) 40–45% quartz, 20–30% plagioclase feldspar, 5–10% alkali feldspar, 5–10% smectite, and 2–5% zeolite, where the zeolite and smectite represent hydrothermal alteration products. ZOB soils are classified as Mollisols and Alfisols. Catchment and hydrometeorological properties for ZOB, LJC, and EFJW are included in Tables 1 and 2.

Most of the precipitation in the site occurs during the winter season and, at higher elevations, primarily as snow. According to prior studies in the East Fork Jemez watershed (Porter, 2012; Perdrial et al., 2014a), snowmelt is the dominant source of "deep" groundwater recharge, as is common in western montane regions (Bales et al., 2006). In this study site, infiltrating snowmelt transports a large seasonal pulse of organic carbon through soil profiles (Perdrial et al., 2012) and into surface water (Perdrial et al., 2014a). Fluorescence spectroscopy studies of DOM in JRB-CZO soils indicate that they comprise a mixture of plant-derived polyphenols, as well as microbial polysaccharides and proteins, with the ratio of plant versus microbial fluorescent components showing seasonal and sorption–desorption dependence (Perdrial et al., 2014a; Vazquez-Ortega et al., 2014).

2.2. Sample collection

Rock samples of porphyritic rhyodacite and zeolitilized Bandelier Tuff were collected in summer 2010 around Redondo Dome in order to span the range of lithologic variation. Soil samples obtained from

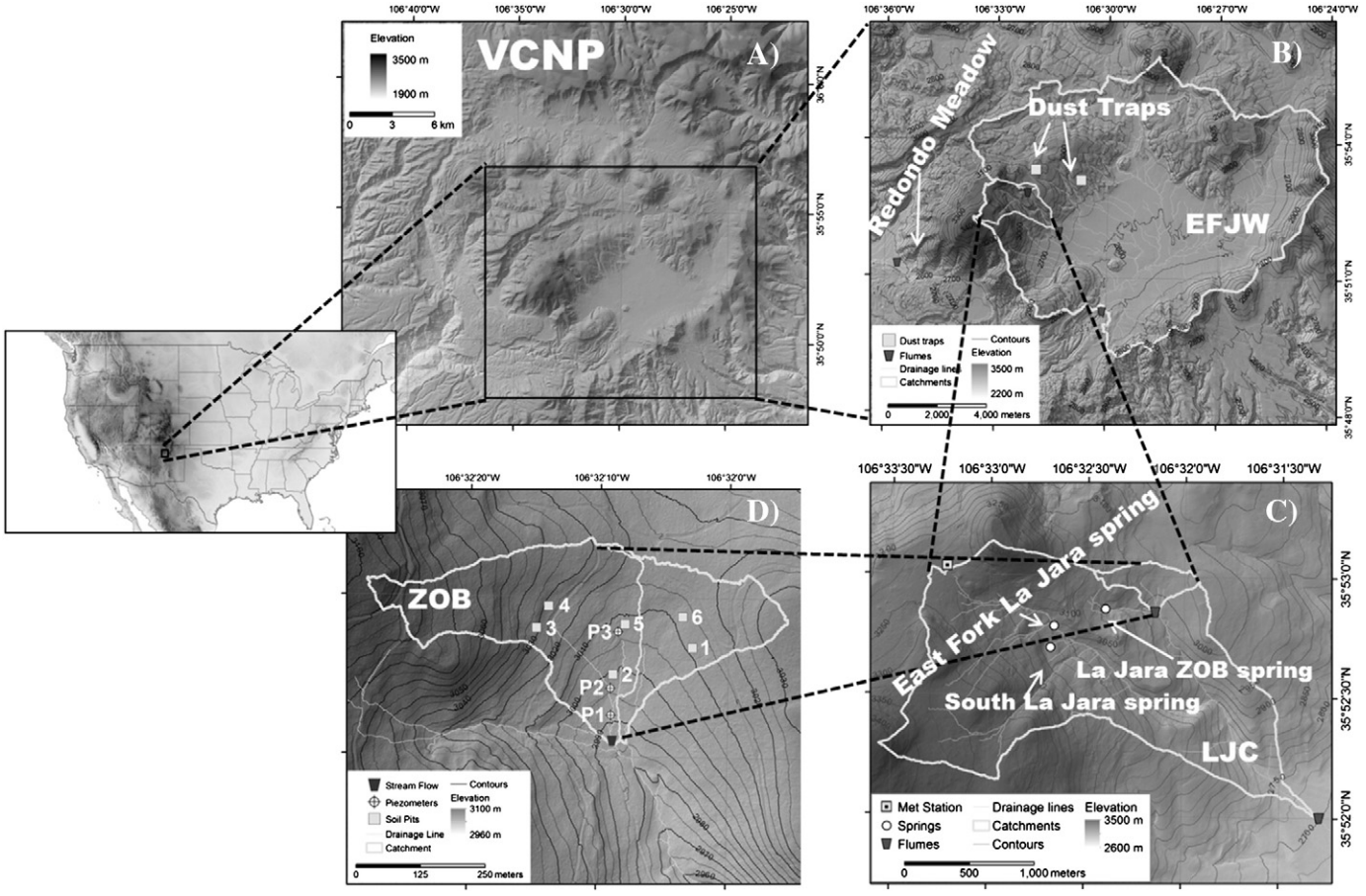

Fig. 1. Overview of JRB CZO field site in the Valles Caldera National Preserve (VCNP) in New Mexico (A). Digital elevation models derived from CZO LiDAR data show landscape locations and nested watershed approach to REY measurements. (B) East Fork Jemez watershed (EFJW) located draining Redondo Mountain and surroundings. (C) La Jara catchment (LJC) and (D) La Jara zero order basin (ZOB) are nested within the larger EFJW. Instrumented pedons (numbered 1–6, installed September 2010) are distributed within the SE and SW facing slopes of the ZOB. Spring sampling, dust trap locations and Redondo Meadow flume are also shown. P1, P2, and P3 correspond to piezometers at 1 (low elevation), 2 (middle elevation), and 3 (high elevation) (D).

six pedons (Fig. 1D) were excavated in La Jara ZOB in September 2010. Soil samples were collected by genetic horizon, composited in the field, sealed in zip-lock bags, and stored at 4 °C. Upon return to the lab, soil materials were air dried, sieved to recover the <2 mm fraction, homogenized, and stored at room temperature.

Atmospheric dust material was collected using field-deployed traps. Traps were constructed from a circular cake pan (area of 450 cm^2) filled with glass marbles and covered with wire mesh (Reheis et al., 1999). The wire mesh was secured with plastic zip-ties. The traps were installed on metal fence posts approximately 1.5 m above ground surface in two locations within the JRB-CZO to assess inputs at higher elevation (3242 m, N 35.88929′ W 106.53234′) and middle elevation (2825 m, N 35.88555′ W 106.51190′) locations within the EFJW watershed (Fig. 1B), with collection from 7/26/11 to 10/15/11. Deionized water was used to rinse marbles and wire mesh for quantitative transfer to 1000 mL bottles. Dust samples were centrifuged and air dried prior to digestion and analysis as discussed below.

Passive capillary wick samplers (PCaps) (Holder et al., 1991; Biddle et al., 1995; Perdrial et al., 2012, 2014b) were used to collect soil solutions as a function of depth in each pedon under a constant negative pressure head of ca. 30 cm (~2.9 kPa). The samplers consist of a fiberglass wick covered with a high density polyethylene (HDPE) plate that is propped via turnbuckles into contact with the bottom of the soil horizon of interest. Liquid samples were guided through tubing into a

Table 1
Physical properties for the three nested study catchments: zero order basin (ZOB), La Jara catchment (LJC), and East Fork Jemez watershed (EFJW). Canopy coverage % was calculated using canopy height >2 m.

Catchment	Area (km^2)	Parent material Fractional contribution		Max discharge (mm/d)[a]			Slope[b] (degrees)	Elevation[b] (meters)	Canopy coverage (%)
		rhyodacite	Bandelier Tuff	WY 2010	WY 2011	WY 2012			
ZOB	0.15	0.47	0.53	no data	17.52[c]	no data	9.0 (0.0–35.1)	3027 (2986–3099)	45.2
LJC	3.67	0.19	0.81	1.5	0.19	0.69	15.8 (0.0–54.6)	3099 (2702–3429)	53.1
EFJW	110.98	0.66	0.34	7.69	0.07	3.70	11.3 (0.0–88.1)	2758 (2582–3432)	36.4

[a] Maximum discharge during the snowmelt period normalized to the catchment area.
[b] Average values are followed by range values in parenthesis.
[c] Predicted max discharge based on a correlation between water content (upper horizon, Pedon 2) and discharge at the outlet of the ZOB.

Table 2
Hydrometeorological data for the water years 2010, 2011 and 2012 in the study site. Measurements are reported from the Redondo station tower and from ultra-sonic snow depth sensor and snow pillow.

Water year	Precipitation (mm)	Depth of max SWE[ab] (mm)	Ambient temperature (°C)[c]	Soil temperature at 5 cm (°C)[c]
2010	680	354	3.26 (−15.70 to 18.90)	5.28 (−1.60 to 15.40)
2011	650	88	3.29 (−25.90 to 17.70)	5.38 (−1.5 to 15.8)
2012	760	278	3.79 (−12.60 to 17.80)	6.33 (0.12 to 16.70)

[a] SWE stands for snow water equivalent.
[b] Snow data obtained from an ultra-sonic snow depth sensor and snow pillow operated by Sandia National Laboratory since 2010, which records snow accumulation and ablation within 500 m of the Valles Caldera flux tower.
[c] Average values are followed by range values in parenthesis for the whole water year.

collection vessel that can be evacuated from the surface. PCaps have been shown to not adsorb, release or fractionate organic matter and REY, and are thus suitable for the present study (Perdrial et al., 2012, 2014b). PCap samples were filtered through 0.7 μm combusted glass fiber filters (unreactive to organic constituents) and stored in acid washed HDPE bottles. Total sample volume was recorded for flux calculations. Soil solutions included in this study were collected in situ during the water years (WY) of 2011 and 2012.

Temperature and water stage were recorded every 30 min at the ZOB and LJC outlets (Fig. 1C–D) with an in-situ level troll 500 and at the EFJW with a Hobo U20 (Fig. 1B). Stage was converted to discharge using a standard equation for Parshall flumes. [A Parshall flume is a widely used open channel flow measurement device, where water flow is contracted and only one depth measurement in the converging section of the flume is required to determine water discharge (Parshall, 1950)]. Only a few water stage measurements at the ZOB during the snowmelt period were recorded due to freezing conditions. In order to obtain discharge measurements from the ZOB, a correlation between volumetric moisture content (at the pedon scale) and discharge was developed and applied during WY 2011; no discharge data was recorded in WY 2012.

Stream water grab samples were collected at flume locations in combusted (475 °C, 4 h) 1000 mL amber glass bottles (for carbon analyses) and 250 mL acid washed HDPE bottles (for metals analyses). Bottles were rinsed three times with stream water, filled to eliminate headspace and stored cool (4 °C) until samples were processed in the lab. Grab shallow groundwater samples were collected following the same protocol as stream water samples during summer and fall seasons of WYs 2011 and 2012. In this study, La Jara ZOB flume, East Fork La Jara spring and South La Jara spring are considered representative of shallow groundwater (Fig. 1D). Redondo Meadow spring was used as a proxy for "deep" groundwater due to: 1) solute concentrations being relatively constant with time; 2) the spring being located at the lowest elevation in our study site; 3) perennial discharge being unresponsive to large precipitation events (snowmelt and monsoon season); 4) tritium concentration analysis and associated dating of the water indicating the longest residence time of springs in the vicinity (*ca.* 14 y with other springs draining Redondo Dome having tritium ages <8 y, unpublished data). Average water table depths at La Jara ZOB for piezometers 1 (P1, low elevation), 2 (P2, middle elevation), and 3 (P3, high elevation) (Fig. 1D) were 1.4 m, 2.2 m and 2.3 m below the land surface, respectively. The highest seasonal variation was observed in P3, where water table depths during the snowmelt period of WY2011 and 2012 were 1.8 m and 0.9 m below the land surface, respectively. Snow samples were collected (i) using a 30 cm snow tube that collects samples integrated across the entire snowpack depth for shallow conditions, (ii) in incremental layers within deeper snowpack, and (iii) using a snow lysimeter. Mean values (n = 65) for snow grab samples collected from 2/13/11 to 5/6/11 are reported here.

For DOC analysis, sample splits were filtered through combusted Whatman 0.7 μm glass fiber filters within 48 h of sampling and filtrate was stored at 4 °C in combusted 60 mL amber glass bottles prior to analysis. For REY analysis, sample splits from the HDPE bottles were filtered through 0.45 μm nylon membranes and stored in 30 mL acid washed HDPE bottles that were acidified to pH 1 with concentrated (16 M) HNO_3. Filtered solutions include both truly dissolved metals and colloidal particles; in this study the term "dissolved" includes both fractions.

2.3. Analytical methods

2.3.1. Solid phase characterizations

Soil samples and unweathered sections of the porphyritic rhyodacite and zeolitilized Bandelier Tuff rocks were analyzed for mineralogical and total elemental composition. Prior to mineralogical determination, organic matter was removed via oxidation using hydrogen peroxide (Jackson, 2005). Mineral composition was determined by quantitative X-ray diffraction at the University of Arizona Center for Environmental Physics and Mineralogy (CEPM) using a PANalytical X'Pert PRO-MPD X-ray diffraction system (PANalytical, Almelo, AA, The Netherlands). Samples were scanned between 5 and 65°2 at a rate of 0.007°2 s^{-1}. Diffractograms were imported into RockJock (Eberl, 2003) with an expanded reference mineral library for quantitation. Particle size composition in soil samples was determined using laser diffractometry (Beckman Coulter LS 13 320) following pretreatment to remove organic matter (Jackson, 2005) (Electronic Annex, Table A.1).

Total elemental concentrations of parent materials and soil samples were measured following lithium metaborate/tetraborate fusion using inductively coupled plasma optical emission spectrometry (ICP-OES) and mass spectrometry (ICP-MS) (Activation Laboratories, Ancaster, Ontario). Recovery of REY for certified standards W-2a (U.S. Geological Survey mafic rock reference) and NCS DC70009 (Tungsten ore) were in the range of 95–105% and 94–104%, respectively. Dust samples were digested in the Arizona Laboratory of Emerging Contaminants (ALEC) using US EPA Method 3052 with HNO_3/HF acids (CEM MDS-2100 microwave digestion system with temperature control). The elemental composition was then determined by ICP-MS (Perkin Elmer DRC II, Shelton, CT). Certified reference materials (CRMs) subjected to the same procedure, including NIST 2702 (Marine sediment) and 2711 (Montana soil), confirmed analyte recovery within the 95–105% range.

2.3.2. Aqueous phase analyses

DOC concentrations were determined using high temperature oxidation followed by infrared detection of CO_2 (Shimadzu TOC-VCSH, Columbia, MD). REY concentrations, as well as those for other metal(loid)s reported here, were determined by ICP-MS equipped with a dynamic reaction cell to eliminate molecular interferences, using matrix matched calibrations and internal standards (Thompson et al., 2006; Goyne et al., 2010). The Perkin Elmer ELAN DRC-II is equipped with NH_3 as an alternate dynamic reaction cell (DRC) gas. Using a typical flow rate of 0.35 mL min^{-1}, the DRC gas was used for Fe-56. Three replicate scans were collected with 40 sweeps per reading. The aqueous CRMs were NIST 1643e (trace metals) and similar "second source" standards from Inorganic Ventures (Christiansburg, VA) and High Purity Standards (Charleston, SC).

2.3.3. REY normalization and anomalies

To enable comparison across the full suite of sample types, REY concentration data for soil and water samples were normalized by a weighted average of CZO rhyolitic bedrock concentrations. Both porphyritic rhyodacite and zeolitilized Bandelier Tuff contribute to the parent rock composition of the site and, therefore, their fresh rock compositions were analyzed for REY concentrations, and the mean REY signatures for ZOB, LJC and EFJW bedrock were calculated from the mapped fractional coverage of the two bedrock types in each catchment (http://geoinfo.nmt.edu/publications/maps/geologic/ofgm/). A mean

REY pattern was generated from a weighted average of porphyritic rhyodacite (0.44) and zeolitilized Bandelier Tuff (0.56) compositions, since that corresponds to the average bedrock composition of the ZOB.

Magnitude of europium and cerium anomalies (Eu / Eu* and Ce / Ce*) was calculated as:

$$\frac{Eu}{Eu^*} = \frac{Eu_{RT}}{(Sm_{RT})^{0.5} \times (Gd_{RT})^{0.5}} \quad (1)$$

$$\frac{Ce}{Ce^*} = \frac{Ce_{RT}}{(La_{RT})^{0.5} \times (Pr_{RT})^{0.5}} \quad (2)$$

where Eu_{RT}, Sm_{RT}, Gd_{RT}, and Pr_{RT} correspond to REE concentrations normalized by the rhyodacite-tuff weighted value. The weighted rhyodacite-tuff average composition is denoted by the subscript "RT". Ratios significantly greater than (less than) 1.0 represent positive (negative) anomalies with respect to rhyodacite-tuff weighted values. In some instances, REY concentrations were normalized to upper continental crust (UCC) (Taylor and McLennan, 1981).

2.3.4. Pedons mass balance calculations

Chemical depletion patterns with depth (tau plots) for soils collected at the ZOB were calculated using the following equation (e.g., Brantley et al., 2007):

$$\tau_{Ti,j} = \frac{C_{a,soil}}{C_{a,parent}} \times \frac{C_{Ti,parent}}{C_{Ti,soil}} - 1 \quad (3)$$

where *Ti* was chosen to represent an 'immobile' element, C_a corresponds to the soil REY concentration, and C_{Ti} is soil Ti concentration. A weighted average parent composition was calculated to provide a single normalization factor representing the aerial distribution of rhyodacite and tuff within each catchment scale of interest. Tau values greater than (less than) zero represent enrichment (depletion) with respect to the RT values.

The fractional contribution to soils of eolian dust (f_d) was calculated based on the method of Ferrier et al. (2011) according to:

$$f_d = \left(\frac{C^P_{Ti}}{C^S_{Ti}} - \frac{C^P_{Zr}}{C^S_{Zr}}\right) * \left[\left(\frac{C^P_{Ti} - C^D_{Ti}}{C^S_{Ti}}\right) - \left(\frac{C^P_{Zr} - C^D_{Zr}}{C^S_{Zr}}\right)\right] \quad (4)$$

where C^P, C^S, and C^D denote concentrations for immobile elements (Ti and Zr) in parent materials (RT), soils, and dust, respectively.

2.3.5. Volume weighted mean concentrations

For soil solutions, volume weighted mean (VWM) concentration values for REY were calculated from:

$$VWM_a = \frac{1}{V_T C_{RT}} \sum_i C_{a,i} V_i \quad \left[mg\,kg^{-1}\right] \quad (5)$$

where *a* corresponds to the REY of interest, $C_{a,i}$ to the concentration of REY for sampling date *i*, V_i is the mass of solution (kg) collected for sampling date *i*, V_T is the total mass of soil solution collected over the snowmelt event, and C_{RT} is the rhyodacite-tuff weighted average for each REY. Discharge values were used for the calculation of VWM concentrations in stream waters.

2.3.6. Geochemical modeling

Geochemical modeling was conducted to assess saturation indices (Ω) of CZ waters with respect to colloidal Fe and Al-(oxyhydr)oxides and cerianite (MINTEQA2 for Windows, Version 1.50, Allison Geoscience Consultants, Inc.). The MINTEQA2 specialized sub-model for aqueous speciation calculations including DOM was included in the calculations. DOC concentration and site density (2.4×10^{-6} mol of sites per mg DOC) were used as input parameters (Susetyo et al., 1991). Saturation indices were employed to predict colloidal gibbsite and goethite and cerianite precipitation or dissolution in the 0.45 μm filtered waters. The Ω value describes quantitatively the relative saturation of an aqueous solution with respect to equilibrium with a solid phase:

$$\Omega = IAP/K_{SO} \quad (6)$$

where IAP is the measured ion activity product corrected for aqueous phase speciation and K_{so} is the solubility product constant for the solid phase.

3. Results

3.1. Characterization of REY sources

JRB-CZO parent rock materials (porphyritic rhyodacite and zeolitilized Bandelier Tuff) show qualitatively similar REY patterns (Fig. 2) when normalized to UCC (Taylor and McLennan, 1981). However, Bandelier Tuff exhibits (i) lower REY concentrations overall ($\sum REY_{UCC} = 15.89$), (ii) a larger negative Eu-anomaly ($[Eu/Eu^*]_{UsCC} = 0.17$) and (iii) smaller concentration increase across the HREE (from Er to Lu) relative to the rhyodacite (Fig. 2, Table 3). Dust samples are depleted in REY relative to both bedrock and UCC ($\sum REY_{UCC} = 8.05$), with a slightly negative Eu-anomaly ($[Eu/Eu^*]_{UCC} = 0.80$) relative to UCC values (Fig. 2, Table 3). The Eu-anomalies in dust samples normalized to RT values range from 1.88 to 2.25 (average = 2.11, n = 3) (Fig. 5).

3.2. REY signatures of groundwater

Shallow groundwater samples were obtained within La Jara catchment (Fig. 1C). The REY_{RT} pattern for La Jara ZOB spring shows high relative HREE concentrations ($[HREE/LREE]_{RT} = 7.7$) (Fig. 3). Similar REY_{RT} values were observed in East Fork La Jara spring ($\sum REY_{RT} = 2.04 \times 10^{-5}$) and South La Jara spring ($\sum REY_{RT} = 1.99 \times 10^{-5}$). Positive Eu-anomalies were observed in all shallow waters; South La Jara spring exhibited the higher positive anomaly ($[Eu/Eu^*]_{RT} = 3.4$). Water at Redondo Meadow spring, which provides a proxy for deep groundwater (Porter, 2012), shows pronounced positive Eu-anomalies ($[Eu/Eu^*]_{RT}$ ranging from 1.04 to 6.80, average = 2.24, n = 18).

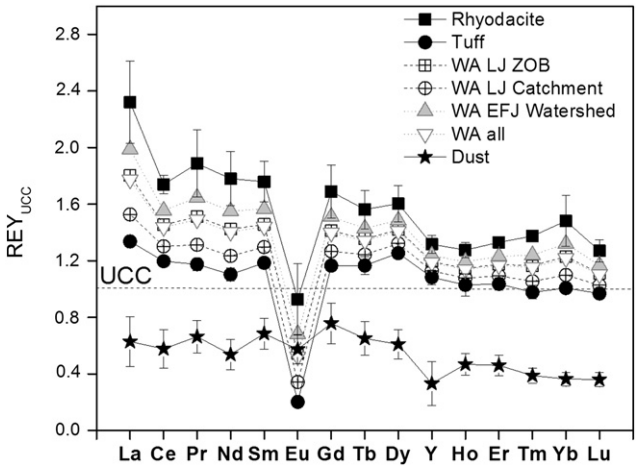

Fig. 2. Rare earth element and yttrium (REY) patterns for parent materials and dust normalized to upper continental crust (UCC) values reported in Taylor and McLennan (1981). Weighted average values (WA) for bedrock in LJ ZOB, LJC, and EFJW (based on fractional area coverage by rhyodacite and tuff) are included for rhyodacite fractions in ZOB, LJC, and EFJW of 0.47, 0.19, and 0.66, respectively. Error bars represent the standard deviation of three replicates.

Table 3
REY values for rhyodacite, Bandelier Tuff, and dust inputs, normalized to UCC and ZOB RT values. P concentrations are reported in mg kg^{-1} and were not normalized.

	Rhyodacite[a]		Tuff[a]		Dust[a]	
	UCC	RT	UCC	RT	UCC	RT
∑REY	23 ± 1	18.3 ± 0.4	15.9 ± 0.2	12.1 ± 0.2	8 ± 2	7 ± 1
LREE/MREE[b]	1.30 ± 0.08	1 ± 0.1	1.29 ± 0.04	1.09 ± 0.03	0.90 ± 0.07	0.61 ± 0.05
LREE/HREE[b]	0.92 ± 0.09	0.73 ± 0.07	0.75 ± 0.01	0.60 ± 0.01	0.90 ± 0.09	1.72 ± 0.07
MREE/HREE[b]	0.71 ± 0.02	0.77 ± 0.02	0.58 ± 0.02	0.55 ± 0.02	1.00 ± 0.03	1.18 ± 0.03
Eu / Eu*	0.6 ± 0.2	1.5 ± 0.6	0.17 ± 0.01	0.45 ± 0.03	0.80 ± 0.08	2.1 ± 0.2
Ce / Ce*	0.8 ± 0.1	1 ± 0.1	0.96 ± 0.02	1.08 ± 0.02	0.89 ± 0.01	1.02 ± 0.02
Phosphorus	262 ± 0		44 ± 0		911 ± 243	

[a] Average values followed by standard deviation, n = 3.
[b] LREE, MREE, and HREE represent light, middle, and heavy rare earth elements, respectively. LREE = La to Nd, MREE = Sm to Tb, HREE = Dy to Lu (Y not included).

3.3. REY signatures of soil solid phase

Depth profiles of soils in the ZOB pedons (locations shown in Fig. 1D) show greater depletion of LREE than HREE relative to parent rock (Fig. 4), exhibiting the depletion trends LREE > MREE ≥ HREE. The REE depletion trends are coherent within a given pedon but vary by pedon and with landscape position. For example, Pedon 1 situated on a planar hillslope location shows decreased depletion with depth (approaching bedrock), whereas Pedon 5 situated in the ZOB hollow (convergent hillslope location) shows the inverse trend.

All horizons exhibit pronounced positive Eu-anomalies with $[Eu / Eu^*]_{RT}$ values ranging from 1.79 to 2.52, mean = 2.18, n = 30 (Fig. 5; also see Fig. A.1 in Appendix for full REY patterns) indicating soil enrichment in Eu relative to the RT signature. Cerium was observed to accumulate in lower horizons in preference to neighboring La and Pr ($[Ce / Ce^*]_{RT}$ from 0.70 to 1.29, average = 1.08, n = 30) (Fig. 6), and soil solutions showed time-dependent changes in Ce anomalies, with positive anomalies at the onset of snowmelt giving way to negative anomalies towards the end of the snowmelt period (Fig. 7, Fig. A.2, Appendix).

3.4. REY signatures of soil pore waters

Soil pore waters in instrumented pedons reveal distinctive REY patterns including pronounced positive Eu anomalies and HREE enrichment (Fig. 7). In Pedon 1 at 3 cm depth (WY2011), a progressive increase in REY concentration was observed towards the end of the snowmelt period. Volume weighted mean values (Table 4) show that REY concentrations are higher in surficial pore waters of Pedon 1, but at depth in Pedon 5, and this observation was consistent in both water years. A prior study showed that water and organic carbon fluxes over the same period were higher in the surface (than at depth) for planar Pedon 1, whereas the inverse was true for the convergent Pedon 5 (Perdrial et al., 2012). This result is consistent with the depletion patterns for these two pedons (Fig. 4), which shows greater solid-phase depletion of REY at the surface for Pedon 1, and at depth for Pedon 5. In addition, soil solutions were preferentially enriched in smaller ionic radius (and hence higher ionic potential) REY (i.e., HREE > MREE > LREE) — a trend that is especially evident for the surface horizons (WY 2011) (e.g., Fig. 7A and B). Similar trends were also observed in Pedon 5 during the WYs 2011 and 2012, Fig. 8).

Soil solutions in the upper horizons of Pedon 1 (WY 2011) exhibited pronounced negative Ce-anomalies during snowmelt (Fig. 7). At 3 cm $[Ce / Ce^*]_{RT}$ ranged from 0.31 to 0.58 with mean = 0.49, n = 6 (Fig. A.2). Conversely, soil solutions at the bottom horizon did not exhibit a Ce fractionation during the first days of the snowmelt, but a negative anomaly developed towards the end of the snowmelt period. For the WY 2012, no trend was observed for Ce fractionation in the bottom horizon (Fig. 7, Fig. A.2).

Correlations between the sum of REE (∑REE) (yttrium not included) and DOC concentrations in soil solutions were weak and insignificant ($p > 0.05$) (WYs 2011 and 2012), (Fig. A.3 and Table A.2). In both pedons, the upper horizons give the highest VWM DOC concentration values (Table 4), but, as mentioned above, unlike planar Pedon 1, convergent Pedon 5 showed higher carbon and water flux at depth (Perdrial et al., 2012; unpublished data). We observed positive correlations between ∑REE and aqueous Al and Fe (WYs 2011 and 2012) (Fig. A.3 and Table A.2). For example, soil solutions collected at 3 and 59 cm in Pedon 1 show strong positive correlations between ∑REE and Al (R^2 = 0.90 and 0.81 for surface and subsurface, respectively), and between ∑REE and Fe (R^2 = 0.92 for the surface horizon, Table A.2).

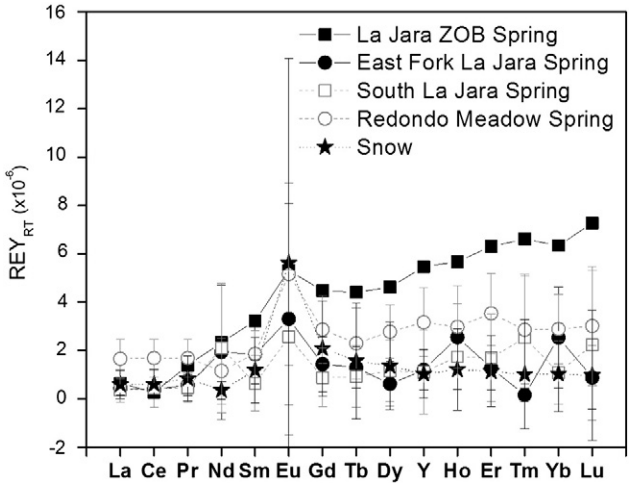

Fig. 3. REY fractionation patterns for shallow and deep groundwater and snow normalized by WA all (shown in Fig. 2). All shallow groundwater samples were collected during summer and fall seasons of WYs 2011 and 2012. In this study, La Jara ZOB spring (n = 1), East Fork La Jara spring (n = 3) and South La Jara spring (n = 5) are defined as shallow groundwater. Mean values (n = 18) are reported for Redondo Meadow spring water (proxy for deep groundwater) collected during the snowmelt period of 2011 and 2012. Mean values (n = 65) are reported for snow grab samples collected during 2/13/11 to 5/6/11. Error bars represent the standard deviation for the corresponding number of samples.

3.5. REY signatures of surface waters

Surface waters draining basins of increasing spatial scale — i.e., ZOB, LJC and EFJW — showed distinct REY signatures, with concentrations being highest for the ZOB outlet (Fig. 9). Solutions collected at the ZOB outlet (WY 2011) were remarkably consistent in REY pattern and significantly enriched in HREE and MREE relative to LREE ($[LREE/MREE]_{RT}$ ranged from 0.34 to 0.43, mean = 0.38, n = 9; $[LREE/HREE]_{RT}$ ranged from 0.19 to 0.29, mean = 0.26, n = 9) (Fig. 10A). A pronounced positive Eu-anomaly ($[Eu / Eu^*]_{RT}$ from 1.61 to 1.68, mean = 1.64, n = 9) was consistently observed at the ZOB scale. ZOB stream water REY patterns were similar to near-surface soil solutions in Pedon 1 at 3 and 24 cm (Fig. 7A and B). Relative to higher order catchments, ZOB stream waters exhibited higher REY concentrations during the initial snowmelt period (after 3/25/11) (Fig. 9).

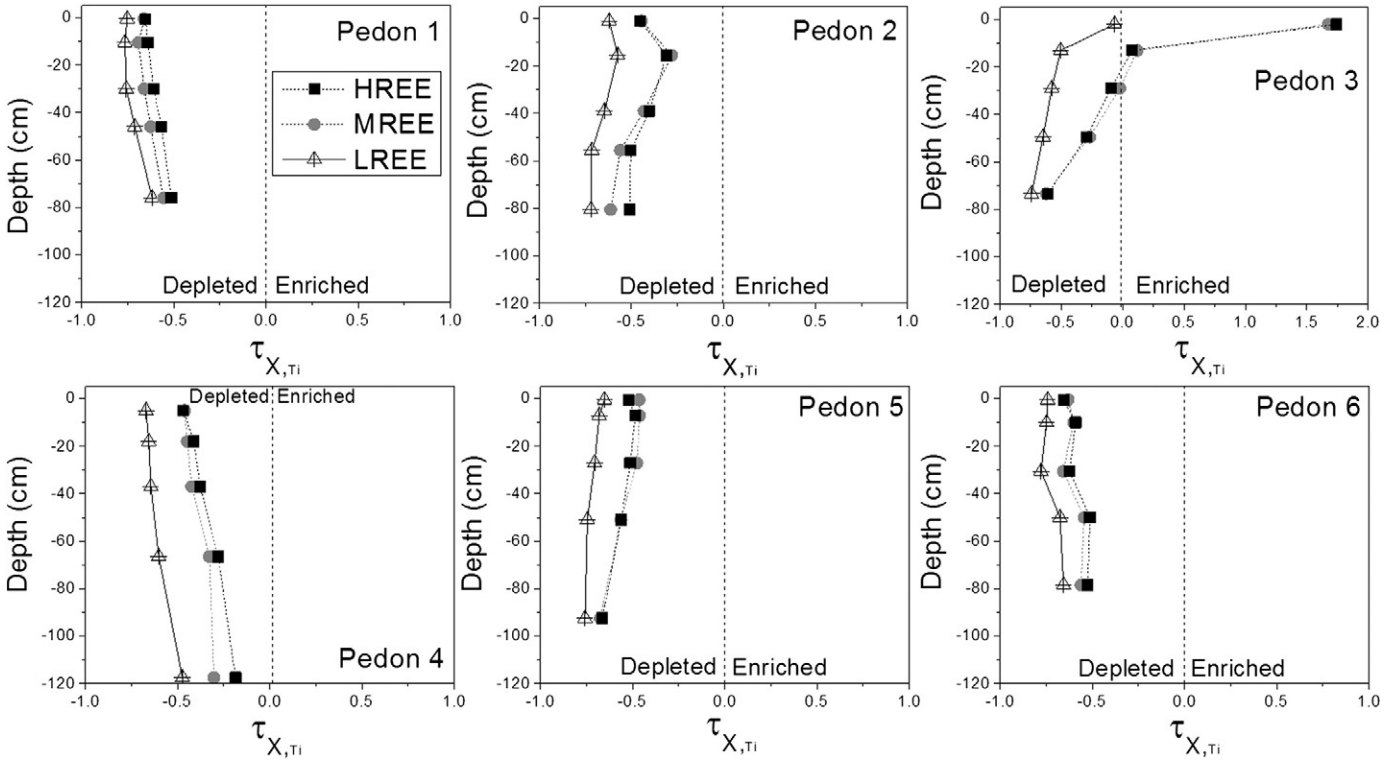

Fig. 4. Chemical depletion (tau value) trends for light, medium and heavy REE as a function of depth for all pedons excavated in the La Jara ZOB with titanium as immobile element, and all values normalized by WA LJ ZOB. Positive tau values represent enrichment and negative values represent depletion with respect to parent materials. In this study LREE (La to Nd), MREE (Sm to Tb), and HREE (Dy to Lu) represent light, middle, and heavy rare earth elements, respectively.

Positive Eu-anomalies were also observed for stream waters in La Jara catchment (WY 2011: average $[Eu / Eu^*]_{RT} = 1.66$; WY 2012: average $[Eu / Eu^*]_{RT} = 1.59$) and East Fork Jemez watershed (WY 2011: average $[Eu / Eu^*]_{RT} = 1.71$; WY 2012: average $[Eu / Eu^*]_{RT} = 2.11$). During the wetter WY 2010, both streams exhibited higher REY concentrations than in 2011 and 2012 (Table 4). Likewise, the volume weighted mean DOC values for La Jara catchment and East Fork Jemez watershed streams were 1.8 and 3.1 times higher during wetter 2010 relative to drier 2011 (Table 4), as discussed in detail elsewhere (Perdrial et al., 2014a).

DOC concentrations increased with discharge for both LJC and EFJW streams, with higher values being observed during the wetter 2010 (Fig. 10A and Table A.3, appendix). High ∑REE concentrations were observed during periods of high discharge in WY 2010, but linear correlations are not significant ($p > 0.05$, Fig. 10B and Table A.3, appendix), following trends similar to DOC. Indeed, ∑REE concentration values are positively correlated with DOC across all catchments during WYs 2010, 2011, and 2012 ($R^2 = 0.80$, $p < 0.01$) (Fig. 10C and Table A.3, appendix). Even stronger ∑REE–DOC correlations are observed for ZOB WY 2011 and EFJ WY 2010 (Table A.3, appendix), each of which

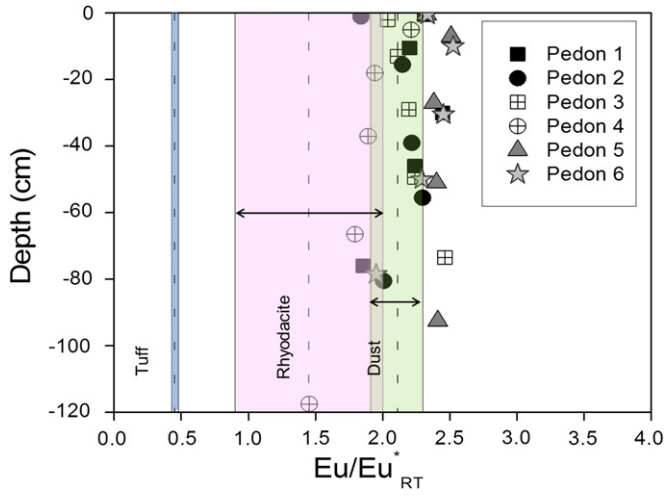

Fig. 5. Eu anomalies for all pedons (all horizons) excavated in La Jara ZOB are plotted with tuff (n = 3), WA LJ ZOB (n = 3), rhyodacite (n = 3), and dust ranges (n = 3). All values were normalized by WA LJ ZOB.

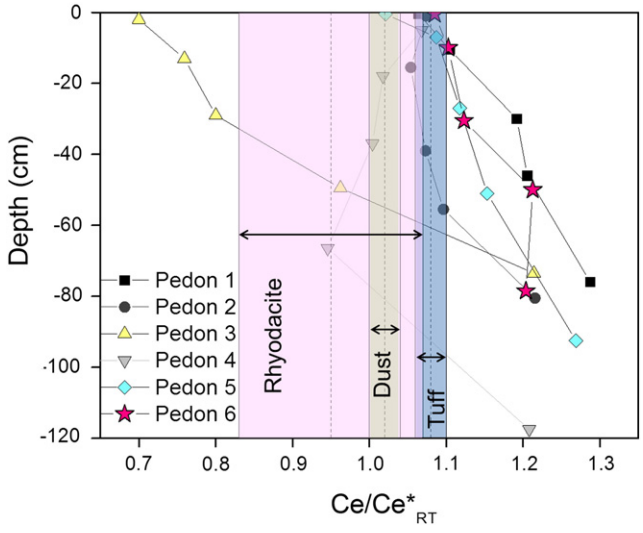

Fig. 6. Quantification of Ce anomalies as a function of depth in all pedons excavated in La Jara ZOB. Range values are reported for tuff (n = 3), rhyodacite (n = 3) and dust (n = 3). All values were normalized by WA LJ ZOB. The differences in the depth dependent trends are statistically significant (p-values less than 0.05) with the exception of Pedons 2 and 4.

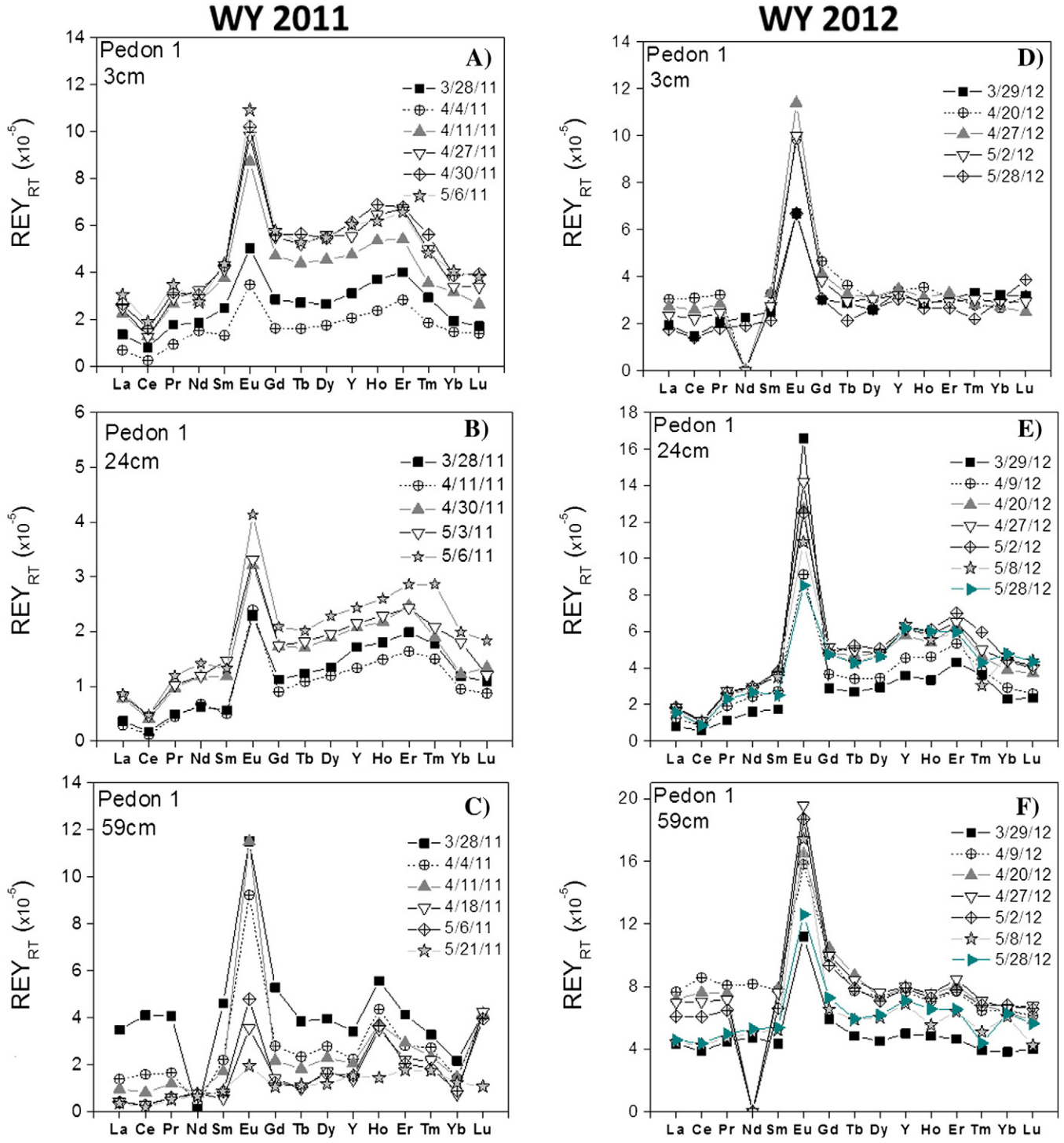

Fig. 7. REY fractionation patterns for soil solutions of Pedon 1 at 3, 24 and 59 cm depth during WYs 2011 and 2012. REY were normalized by WA All values. Note differences in y-axis scales.

provides a wide range in both REE and DOC concentrations. As with soil pore waters (above), ∑REE concentrations in surface waters are positively correlated with those of dissolved Al and Fe (Table A.4, Appendix).

4. Discussion

4.1. Influences of biogeochemical weathering processes on REY across scales

Coherent REY trends were observed in this study across a range of temporal (hydrologic event to pedogenic) and spatial (pedon to ZOB to catchment to watershed) scales. Aqueous REY patterns represent a relatively consistent fingerprint for a given location in the landscape, but with a magnitude (normalized concentrations) impacted by sampling time. The data suggest that partitioning of REY between solid matrix and aqueous phases is driven by event-based dynamics of DOC and colloidal materials. In the case of the JRB-CZO site, where "deep" groundwater recharge is dominantly by snowmelt, pulsed water and carbon influx to the subsurface occur during a period of rapidly increasing photosynthesis and net ecosystem uptake of CO_2 driven by water availability, a pattern that also impacts soil pore water chemistry and streamflow during and following snowmelt (Perdrial et al.,

Table 4
Volume weighted mean values (VWMs) for DOC and normalized ∑REY concentrations during the snowmelt event. Soil solution data was obtained during WYs 2011 and 2012. Surface water data was obtained during WYs 2010, 2011 and 2012.

	Site, location, year		DOC[a] (mg/L)	VWM for DOC (mg/L)	∑REY[a] (mg/L)	VWM for ∑REY (mg/L)
Pedon 1,	3 cm	WY 2011	24.0–63.0	40.7	2.5×10^{-4}–7.1×10^{-4}	6.9×10^{-4}
Soil solution		WY 2012	2.6–18.6	6.1	4.1×10^{-4}–5.3×10^{-4}	4.5×10^{-4}
	59 cm	WY 2011	15.7–30.2	17.6	1.7×10^{-4}–6.4×10^{-4}	4.8×10^{-4}
		WY 2012	1.4–22.4	11.4	7.4×10^{-4}–1.2×10^{-3}	1.0×10^{-3}
Pedon 5,	5 cm	WY 2011	23.1–35.9	26.5	8.8×10^{-5}–1.5×10^{-4}	1.4×10^{-4}
Soil solution		WY 2012	2.94–35.7	24.5	1.4×10^{-3}–1.9×10^{-3}	1.5×10^{-3}
	54 cm	WY 2011[b]	9.8	9.8	4.7×10^{-4}	4.7×10^{-4}
		WY 2012	1.1–10.9	9.9	3.6×10^{-4}–5.1×10^{-4}	4.4×10^{-4}
La Jara ZOB		WY 2011	5.1–12.1	10.0	2.6×10^{-4}–7.7×10^{-4}	7.2×10^{-4}
La Jara catchment		WY 2010	1.8–5.2	3.8	3×10^{-5}–2.3×10^{-4}	1.8×10^{-4}
		WY 2011	1.7–2.8	2.1	3.4×10^{-5}–6.8×10^{-5}	5.9×10^{-5}
		WY 2012	3.0–5.1	4.1	6.3×10^{-5}–1.2×10^{-4}	4.1×10^{-5}
EFJ watershed		WY 2010	2.9–14.1	10.2	8.1×10^{-5}–5.8×10^{-4}	4.2×10^{-4}
		WY 2011	1.3–6.8	3.2	8.1×10^{-5}–1.7×10^{-4}	1.2×10^{-4}
		WY 2012	3.7–12.3	9.9	4.6×10^{-5}–2.3×10^{-4}	1.9×10^{-4}

[a] Range for DOC and ∑REY concentrations in soil solutions and stream waters.
[b] n = 1, for Pedon 5 at 54 cm during the snowmelt event WY 2011.

2014a). Snowmelt-generated DOC throughflux affects REY removal from soil profiles (e.g., Fig. 4 and related text), metal-DOC complex release into surface waters (Fig. 10C), and hence the impacts of REY chemical denudation in rhyolitic terrain. As discussed below, when viewed in light of prior work, results of this study suggest that weathering of REY in the CZ is strongly dependent on the coupling of seasonal water availability to landscape biotic activity, which imprints a signature in both mobile solutions (Figs. 3, 7–10, A.3, A.4) and regolith (Figs. 4, 5, A.1, A.2). In the rhyolitic EFJW watershed, mechanisms controlling REY transport and fate in soil, ground and stream waters include (1) weathering of primary phosphate and silicate minerals, (2) aqueous and solid phase complexation with organic matter, (3) adsorption and co-precipitation with secondary minerals, (4) colloid formation and transport and (5) inorganic complexation (e.g. sulfate, carbonate, and hydroxide ligands) (Wood, 1990; Byrne and Li, 1995; Tang and Johannesson, 2003; Sonke and Salters, 2006; Pourret et al., 2007a and b; Tang and Johannesson, 2010a).

Phosphate minerals such as apatite or monazite can partially control the REY budget in soils, soil solutions, and stream waters (Aubert et al., 2001; Tang and Johannesson, 2003; Stille et al., 2009), and their rates of dissolution are impacted by organic acids present in soil solutions. For example, low molecular weight organic acids (LMWOAs) such as citrate, oxalate, and phthalate can enhance phosphate mineral weathering and alter the stoichiometry of mineral REE release (Goyne et al., 2010). At the various landscape scales of interest in the EFJW, ligand-promoted REY dissolution mechanisms are most active during water and DOC throughflux events, and water and carbon CZ through-fluxes are dominated by winter snowmelt (Perdrial et al., 2014a). Both the parent rock and influent dust contain substantive total phosphorus (Table 3), which can be associated with phosphate and alkali feldspar minerals (Nash, 1984; London, 1992). Hence, dust inputs may contribute significantly to near surface REY measurements. Eolian fractions (f_d) for the ZOB soils calculated using Ti and Zr as immobile elements according to Ferrier et al. (2011) (Table A.6, electronic annex) indicate that the upper horizons have a greater elemental fraction from dust deposition. Importantly, when normalized to the RT, dust exhibits the largest positive Eu-anomaly of potential sources and appears to move soil pedon values in that direction as well (Fig. 5). It is noteworthy that total soil phosphorus was positively correlated with MREE and also (but less so) with HREE (data not shown), consistent with phosphate mineral enrichment in MREE. Prior studies have also shown MREE enrichment in soil organic matter (Tang and Johannesson, 2010a), and some of the total P is certainly organic as well. Total phosphorus in ZOB stream water exhibits a positive correlation with ∑REE, consistent with REE system fluxes being at least partially controlled by phosphate mineral dissolution (Table A.4, Appendix). The least REY depleted soils were those with the highest clay content (correlations not shown), suggesting that precipitation of secondary minerals diminishes REY removal from the weathering profile (Fig. 4, Pedons 1, 2, 3, and 6). While this effect is certainly due, in part, to Fe and Al (oxy)hydroxide formation, cation exchange capacity (CEC) associated with layer silicate clays is also predictive of REY adsorptive retention in soils (Coppin et al., 2002).

Soil solutions and stream waters at the ZOB outlet exhibited higher REE and DOC concentrations than stream waters draining the larger LJC and EFJW (WY 2011) (Table 4). High aqueous REE concentrations and mobilization in soil pore waters and at the ZOB outlet can be attributed to dissolution and/or dispersion of Al, Fe-(oxy)hydroxide colloids, promoted in part by the formation of mobile REE-DOM complexes. However, the role of organic matter is complex because, despite the fact that soil solutions contain large amounts of DOC (concentration ranges from 15 to 60 mg L^{-1}), weak correlations were observed between DOC and ∑REE alone, and stronger ones were observed for ∑REE and total filterable Al and Fe (Fig. A.3, Appendix). This suggests that Fe and Al-(oxy)hydroxide colloids — which are continuously formed in soil pores during incongruent weathering — are mobile carriers of REE in pore waters. In so far as these particles are preferentially mobilized (particularly when they are negatively-charged as a result of OM adsorption, e.g., Chorover and Sposito, 1995; Thompson et al., 2006), they appear to be important vectors for catchment geochemical denudation, though most studies pay little attention to this transport mechanism.

Since colloidal forms of REE would be included in the "dissolved" pool as measured following filtration, we conducted geochemical modeling to find that analyzed solutions were indeed supersaturated with respect to Al and Fe-(oxy)hydroxides. Saturation index calculations were conducted following aqueous phase speciation that included the effects of complexation with DOM. The results indicated that precipitation of Al and Fe (oxy)hydroxides is predicted thermodynamically (Table A.5, Appendix), and colloidal forms were likely present in our pore water filtrate solutions. Such materials are likely important to the development of depletion profiles in pedogenic environments, e.g., fine clays enriched in Fe-(oxy)hydroxides, kaolinite, and gibbsite were the primary mobile colloids in reconstructed pedons (Kaplan et al., 1997). We assert that organo-mineral colloid transport is important to REE redistributions at the pedon and hillslope scale in the JRB-CZO site as well.

At the ZOB scale (WY 2011), a strong positive correlation between ∑REE and DOC was observed, and REE mobilization could be largely explained by DOM complexation (Fig. 10C). The influence of OM is therefore persistent across all of our measurements, suggesting a strong role for biological mediation of REE chemical denudation from rock to

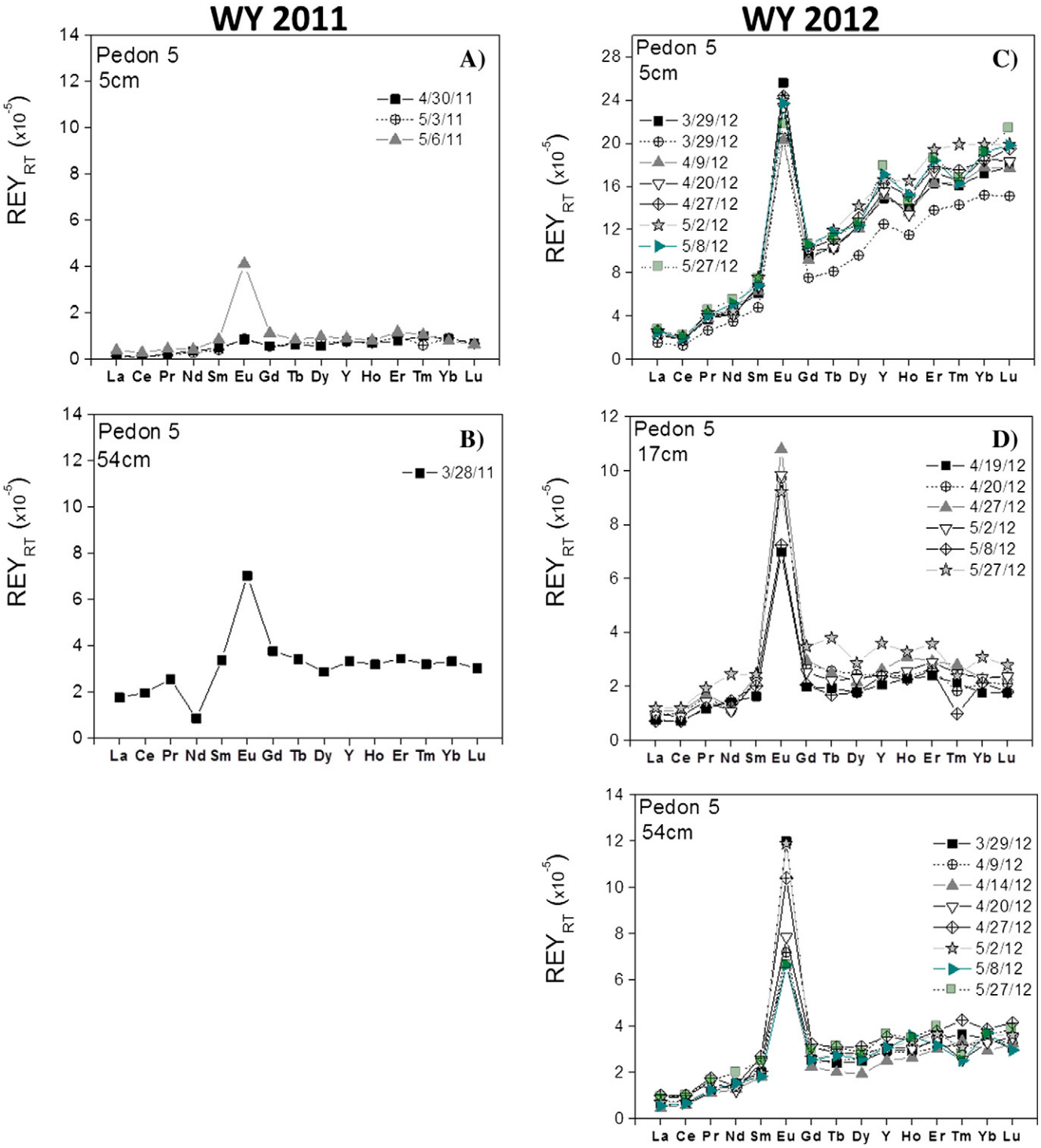

Fig. 8. REY fractionation patterns for soil solutions of Pedon 5 at 5 and 54 cm depth during the WYs 2011 and 2012. REY were normalized by WA all values. Note differences in y-axis scales.

soil to soil solution to stream waters, and these data are consistent with prior reports. For example, application of the Humic Ion-Binding Model V likewise indicated that REE concentrations were controlled dominantly by their DOM complexation in natural fresh waters (Johannesson et al., 2004).

During the WY 2012, DOC and ∑REE concentrations in stream waters at LJC were positively correlated with discharge (Fig. 10). In contrast, a poorer correlation was observed for drier WY 2011, suggesting that DOC and associated REE mobilization from catchment soils are strongly dependent on hydrologic fluxes that are, in turn a function of snowpack accumulation and snow water equivalent (Perdrial et al., 2014a). Weaker correlations between DOC and ∑REE during WY 2011 (Fig. 10C) are attributed to the low water flux in 2011, also highlighting the fact that it is concurrent delivery into the weathering zone of high DOC concentrations and geochemically aggressive freshwater that drives the chemical denudation of organic-ligand-reactive lithogenic metals.

Colloidal transport is also implicated in REE mobilization in LJC and EFJW surface waters, as indicated by a positive correlation with Al and Fe concentrations during the intermediate water year 2012 (Table A.4, Appendix). Sholkovitz (1992) conducted sequential filtrations on stream waters (pore sizes of 0.45, 0.2, and 0.025 μm)

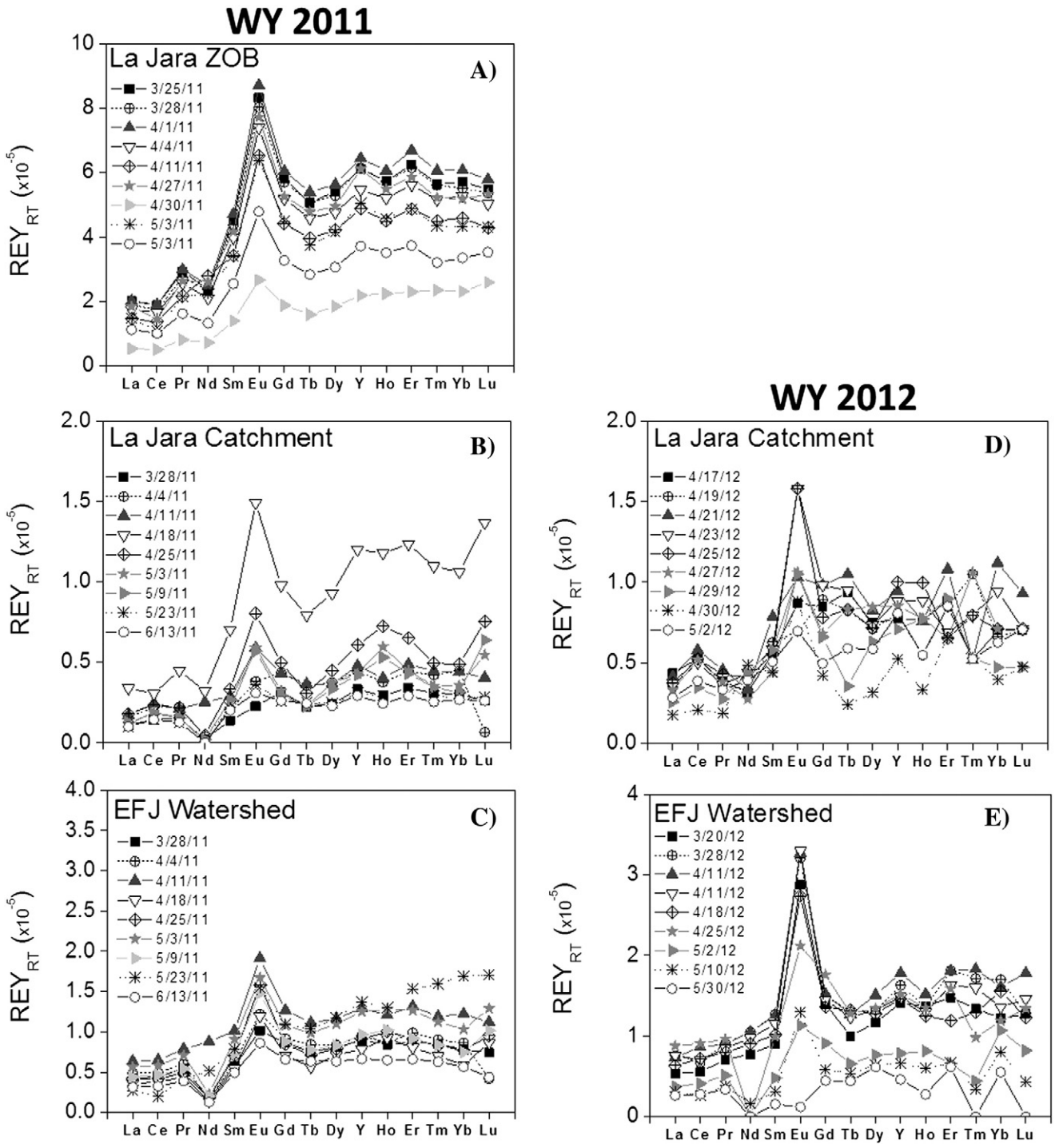

Fig. 9. REY fractionation patterns for stream waters at the outlet of La Jara ZOB, La Jara catchment, and EFJ watershed during the WYs 2011 and 2012. REY were normalized by WA All. Note differences in y-axis scales.

and concluded that a large portion of REE was in the colloidal load, indicating that colloids can control REE distribution in stream waters.

For DOC and colloidal carriers to dominate REE transport in our study site, they must play a larger role than inorganic ligands (e.g. sulfate, carbonate, and hydroxide ligands) that can also form complexes with REE in natural waters (Wood, 1990; Byrne and Li, 1995; Tang and Johannesson, 2003; Sonke and Salters, 2006; Pourret et al., 2007a and b; Tang and Johannesson, 2010a). Indeed, an evaluation of our data in light of prior work supports this contention. Specifically, a comparison of major and trace ion chemistry between world average river water (Livingstone, 1963; Martin and Meybeck, 1979; Tang and Johannesson, 2003; Pourret et al., 2007a) and JRB-CZO solutions was employed to assess the relative role of inorganic ligands in REE complexation in our study site (see Appendix). During the periods of study, JRB-CZO solutions exhibited lower inorganic carbon (as HCO_3), SO_4, Cl, and NO_3 concentrations than world average river water, but very similar DOC concentrations and pH. For example, the mean HCO_3, SO_4, Cl, and NO_3 concentrations (in mg L^{-1}) for LJC in WY 2010 were 3.3, 2.8, 8.5, and 1.8 times lower than world average river data, respectively. Despite the higher inorganic ligand concentrations for world average river water, speciation modeling results indicated that the

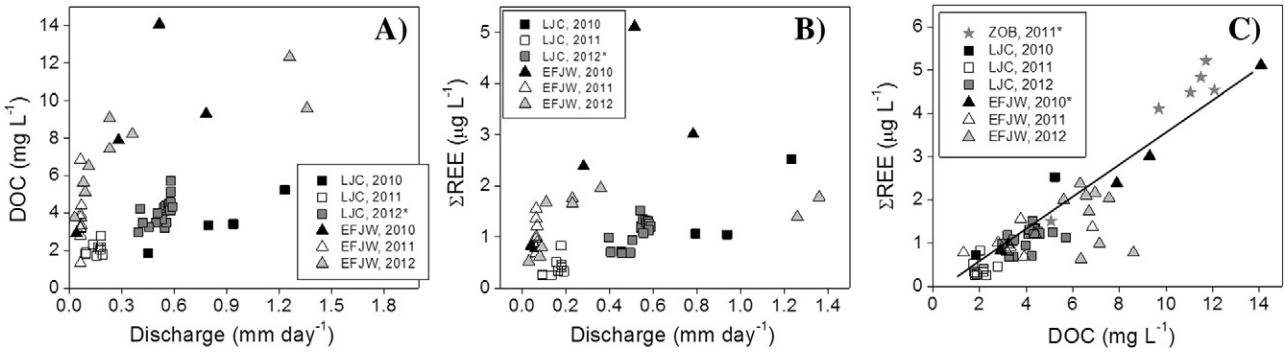

Fig. 10. Relations between (A) Discharge versus DOC, (B) discharge versus ∑REE, and (C) DOC versus ∑REE for surface waters at the outlet of nested catchment series (ZOB, La Jara catchment, and East Fork Jemez watershed) during the snowmelt period for WYs 2010, 2011, and 2012. The coefficient of determination (R^2) for the entire data set in part C is 0.80. REEs are in mg L^{-1} (not normalized). Asterisk (*) indicates cases where the correlation is significant ($p < 0.05$) (also see Table A.3).

majority of REEs (>50%) in those solutions were nonetheless complexed with DOM, and that a low percentage of REE could be allocated to SO_4 (<20% at acidic pH) and CO_3 (<40% at alkaline pH) complexes (Pourret et al., 2007a). Given the lower concentration of inorganic ligands and similar DOC concentrations in JRB-CZO solutions relative to world average river waters, the inorganic contribution to REE complexation is smaller at our site. It is noteworthy that Al concentrations in JRB-CZO surface waters are 3–4 fold higher than that in the world average river water, suggesting potential competition with REE for DOM active sites, but as indicated earlier much of this Al is likely in colloidal form. In any case, further research into REE aqueous speciation of JRB-CZO waters is warranted; direct speciation measurements are needed to quantify unambiguously the fractional abundance of REE-DOM complexes.

4.2. Eu-anomaly: an indicator of REE sources?

Among the patterns observed in the current study were pronounced positive Eu-anomalies in the soil matrix, soil solutions, and stream waters (Figs. 5–9 and A.1, Appendix). While several processes can potentially contribute to the positive Eu-anomaly, we attribute the observations in our site to dust deposition superimposed with preferential weathering of feldspar minerals. Dust deposition inputs contribute to Eu enrichment in bulk soil solids (Fig. 5) because dust is less depleted in Eu than parent rock (Fig. 2, Table 3). Indeed, mass balance calculations indicate significant eolian contributions to soil, particularly in the upper horizons (Table A.6, Appendix). Dust dissolution should then supplement any positive Eu anomalies of soil solutions and stream waters deriving from preferential feldspar dissolution. Over pedogenic time scales, Eu accumulation from dust plus preferential feldspar dissolution could together induce the positive Eu-anomaly observed in both soils and natural waters in our study site. Dust inputs are delivered by southerly winds (http://www.wrcc.dri.edu/htmlfiles/westwinddir.html) with sources deriving from low-vegetation-cover geomorphic surfaces of the Rio Grande Valley and playas of the Chihuahuan Desert. Consistent with the results presented here, prior REE and isotopic studies have also shown that pore waters and upper soil horizons can reflect the significant contributions of atmospherically-derived REEs (Aubert et al., 2002; Stille et al., 2009).

Feldspar minerals are enriched in Eu (relative to other REEs) because during primary mineral crystallization and growth from magma devoid of dioxygen, Eu^{2+} substitutes into Ca^{2+}, Na^{+}, and K^{+} sites similar to Sr^{2+} (Aubert et al., 2001). Porphyritic rhyodacite and Bandelier Tuff contain a large percentage of plagioclase (albite and oligoclase) and alkali feldspar (sanidine) (Section 2.1). When these rocks undergo surficial weathering in oxic environments, Eu^{2+} is released and readily oxidized (Panahi et al., 2000). Several studies (Ma et al., 2011; Brioschi et al., 2013) have reported positive Eu-anomalies in soils and natural waters (pore and stream waters), and attributed this to the preferential weathering of feldspar minerals.

4.3. Ce-anomaly: a potential indicator for redox conditions in the ZOB soils

In our study site (also in Braun et al., 1990), soils exhibited a preferential accumulation of cerium with depth (Fig. 6). Redox conditions can influence the development of such cerium (Ce) anomalies because of Ce(III) to Ce(IV) oxidation (Feng, 2010; Laveuf et al., 2012), which occurs at Eh values of *ca.* 300 mV for circumneutral pH (Ronov et al., 1967; Laveuf and Cornu, 2009). Tetravalent Ce is characterized by especially low mobility due to the low solubility of cerianite (CeO_2) and strong interaction (via adsorption and/or coprecipitation) of Ce(IV) with Fe- and Mn-oxides (Laveuf, et al., 2008; Feng, 2010). The Ce-anomaly trends in our study (Fig. 6) are clearly attributable to pedogenic processes, since the Ce-anomalies for parent rock (RT) and dust sources are both much lower to those observed at depth in soil horizons (Fig. 6). Linear regression analysis indicates depth dependent trends that are statistically significant ($p < 0.05$) for Pedons 1, 3, 5 and 6, but not for Pedons 2 and 4 where the trends are more non-linear and complex (Fig. 6). Several studies (Bau, 1999; Bau and Koschinsky, 2009) have demonstrated that Ce(III) is oxidized by surface reaction and electron transfer to Fe(III)- and Mn(IV) in secondary (oxy)hydroxides. De Carlo and Wen (1998) demonstrated (first proposed by Goldberg et al., 1963) that Ce is exclusively decoupled from trivalent REE by abiotic oxidation by Mn-oxides.

The solid phase trends can be interpreted in light of observed time series in solution phase chemistry. Specifically, the change in Ce-anomaly at depth in Pedon 1 (for the soil waters, WY 2011, Fig. 7c) is consistent with a progressive change in redox conditions from reducing to oxidizing over the course of the snowmelt period, likely resulting from a seasonal fluctuation in the groundwater table, which imposes a potentially steep redox gradient (also see Fig. A.2, Appendix). Soils with low water saturation remain oxic favoring Ce(IV) precipitation and negative Ce-anomalies in soil solution, whereas high water saturation disfavors Ce(III) oxidation. The likelihood of cerianite precipitation was assessed by geochemical modeling (MINTEQA2) and all analyzed solutions were found supersaturated with respect to cerianite at atmospheric partial pressure of O_2 (Table A.5, Appendix). Conversely, high and prolonged soil water saturation likely induces reducing conditions that favor reduction of Ce(IV) to Ce(III), release of Ce to soil solution, and positive aqueous Ce anomalies as Ce(IV) enriched redox-active solids (e.g., Mn(IV) or Fe(III) oxides) undergo reductive dissolution. Chemical processes influencing Ce concentrations at the oxic/anoxic marine interface in the Cariaco Trench have been study by DeBaar et al. (1988). That study showed that filtered oxic seawater was supersaturated with respect to cerianite despite negative Ce-anomalies, indicating Ce removal via precipitation from the water column. Conversely, the anoxic region exhibited a slightly positive Ce-anomaly. In summary, the results of the present work indicate that Ce-anomalies in critical

zone porewaters can serve as useful indicators of redox conditions and associated dynamics during hydrologic events.

5. Conclusions

REE distribution patterns in weathering soil profiles and mobile solutions are consistent with fractionation across the lanthanide series during variable release from primary minerals and differential re-precipitation in secondary (organo-)mineral complexes. REE fractionation resulted in an HREE enrichment in streamwaters, consistent with a strong correlation between REE with DOC concentrations, and a prevalence of organo-REE complexes. These results signal a strong role for biotic mediation of REE chemical denudation, and that REEs are reactive tracers of biological weathering. Soluble organic matter does not exert the sole control over REE fractionation; the data also indicate an important effect of Fe and Al-(oxy)hydroxides colloids as mobile sorbents for REE (and therefore probably other trace metals as well). But even in this case, surface complexation of natural organic matter is expected to enhance the mobilization of such colloids in the weathering profile by enhancing their negative surface charge.

The presence of positive Eu-anomalies in regolith can be attributed to dust deposition as indicated by a substantive eolian fraction (decreasing with depth) that is enriched in Eu relative to parent rock. Positive Eu anomalies in pore water solutions and stream waters are attributed to dissolution of that dust as well as preferential dissolution of feldspars derived from the rhyolitic parent material.

Cerium anomalies in both soils and pore waters are observed to be related to spatially and temporally varying redox status, with reducing conditions dominantly associated with the pulsed release to soils of water with high DOC concentration early in snowmelt. Negative Ce-anomalies in pore waters can be used as a proxy for oxic conditions because of adsorption/co-precipitation of Ce(IV) with Fe and Mn oxides or cerianite precipitation. Conversely, during initial snowmelt when soils are water saturated and DOC concentrations are high, pore waters yield $[Ce / Ce^*]_{RT} \geq 1$, indicating microbially-active, sub-oxic conditions wherein Ce(III) oxidation is precluded, and reductive dissolution of Ce(IV) from secondary mineral forms is enhanced.

Acknowledgments

This research was funded by the U.S. National Science Foundation grants EAR-0724958 and EAR-1331408 provided in support of the Catalina-Jemez Critical Zone Observatory and EAR/IF-0929850. Thanks to Scott Compton, Caitlin Orem, Mercer Meding, and Courtney Porter for assistance with sampling and analysis. Thanks to Matej Durcik for help with the JRB-CZO GIS system.

Appendix A. Supplementary data

Supplementary data to this article can be found online at http://dx.doi.org/10.1016/j.chemgeo.2014.10.016.

References

Aubert, D., Stille, P., Probst, A., 2001. REE fractionation during granite weathering and removal by waters and suspended loads: Sr and Nd isotopic evidence. Geochim. Cosmochim. Acta 65, 387–406.

Aubert, D., Stille, P., Probst, A., Gauthier-Lafaye, F., Pourcelot, L., Del Nero, M., 2002. Characterization and migration of atmospheric REE in soils and surface waters. Geochim. Cosmochim. Acta 66, 3339–3350.

Bailey, S., Mayer, B., Mitchell, M., 2004. Evidence for influence of mineral weathering on stream water sulphate in Vermont and New Hampshire (USA). Hydrol. Process. 18, 1639–1653.

Bales, R.C., Molotch, N.P., Painter, T.H., Dettinger, M.D., Rice, R., Dozier, J., 2006. Mountain hydrology of the western United States. Water Resour. Res. 42, W08432.

Bau, M., 1999. Scavenging of dissolved yttrium and rare earths by precipitating iron oxyhydroxide: experimental evidence for Ce oxidation, Y-Ho fractionation, and lanthanide tetrad effect. Geochim. Cosmochim. Acta 63, 67–77.

Bau, M., Koschinsky, A., 2009. Oxidative scavenging of cerium on hydrous Fe oxide: evidence from the distribution of rare earth elements and yttrium between Fe oxides and Mn oxides in hydrogenetic ferromanganese crusts. Geochem. J. 43, 37–47.

Biddle, D.L., Chittleborough, D.J., Fitzpatrick, R.W., 1995. Field monitoring of solute and colloid mobility in a gneissic sub-catchment, South Australia. Appl. Clay Sci. 9, 433–442.

Brantley, S.L., Goldhaber, M.B., Ragnarsdottir, K.V., 2007. Crossing disciplines and scales to understand the critical zone. Elem. 3, 307–314.

Braun, J., Pagel, M., Muller, J., Bilong, P., Michard, A., Guillet, B., 1990. Cerium anomalies in lateritic profiles. Geochim. Cosmochim. Acta 54, 781–795.

Braun, J.J., Viers, J., Dupre, B., Polve, M., Ndam, J., Muller, J.P., 1998. Solid/liquid REE fractionation in the lateritic system of Goyoum, east Cameroon: the implication for the present dynamics of the soil covers of the humid tropical regions. Geochim. Cosmochim. Acta 62, 273–299.

Brioschi, L., Steinmann, M., Lucot, E., Pierret, M.C., Stille, P., Prunier, J., Badot, P.M., 2013. Transfer of rare earth elements (REE) from natural soil to plant systems: implications for the environmental availability of anthropogenic REE. Plant Soil 366, 143–163.

Brooks, P.D., Vivoni, 2008. Mountain ecohydrology: quantifying the role of vegetation in the water balance of montane catchments. Ecohydrol. 1, 187–192.

Byrne, R., Li, B., 1995. Comparative complexation behavior of the rare-earths. Geochim. Cosmochim. Acta 59, 4575–4589.

Chorover, J., Sposito, G., 1995. Colloid chemistry of kaolinitic tropical soils. Soil Sci. Soc. Am. J. 59, 1558–1564.

Chorover, J., Troch, P.A., Rasmussen, C., Brooks, P.D., Pelletier, J.D., Breshars, D.D., Huxman, T.E., Kurc, S.A., Lohse, K.A., McIntosh, J.C., Meixner, T., Schaap, M.G., Litvak, M.E., Perdrial, J., Harpold, A., Durcik, M., 2011. How water, carbon, and energy drive critical zone evolution: the Jemez-Santa Catalina Critical Zone Observatory. Vadose Zone J. 10, 884–899.

Coppin, F., Berger, G., Bauer, A., Castet, S., Loubet, M., 2002. Sorption of lanthanides on smectite and kaolinite. Chem. Geol. 182, 57–68.

Davranche, M., Pourret, O., Gruau, G., Dia, A., 2004. Impact of humate complexation on the adsorption of REE onto Fe oxyhydroxide. J. Colloid Interface Sci. 277, 271–279.

Davranche, M., Pourret, O., Gruau, G., Dia, A., Le Coz-Bouhnik, M., 2005. Adsorption of REE(III)-humate complexes onto MnO2: experimental evidence for cerium anomaly and lanthanide tetrad effect suppression. Geochim. Cosmochim. Acta 69, 4825–4835.

Davranche, M., Grybos, M., Gruau, G., Pedrot, M., Dia, A., Marsac, R., 2011. Rare earth element patterns: a tool for identifying trace metal sources during wetland soil reduction. Chem. Geol. 284, 127–137.

De Carlo, E., Wen, X., 1998. The influence of redox reactions on the uptake of dissolved Ce by suspended Fe and Mn oxide particles. Aquat. Geochem. 3, 357–389.

DeBaar, H., German, C., Elderfield, H., Vangaans, P., 1988. Rare-earth element distributions in anoxic waters of the Cariaco Trench. Geochim. Cosmochim. Acta 52, 1203–1219.

Dupre, B., Viers, J., Dandurand, J., Polve, M., Benezeth, P., Vervier, P., Braun, J., 1999. Major and trace elements associated with colloids in organic-rich river waters: ultrafiltration of natural and spiked solutions. Chem. Geol. 160, 63–80.

Eberl, D.D., 2003. User's Guide to RockJock — A Program for Determining Quantitative Mineralogy From Powder X-ray Diffraction Data. U.S. Geological Survey Open-File Report 2003, (78, 47 p).

Elderfield, H., 1988. The oceanic chemistry of the rare-earth elements. Philos. Trans. R. Soc. A Math. Phys. Eng. Sci. 325, 105–126.

Elderfield, H., Upstillgoddard, R., Sholkovitz, E., 1990. The rare-earth elements in rivers, estuaries, and coastal seas and their significance to the composition of ocean waters. Geochim. Cosmochim. Acta 54, 971–991.

Feng, J., 2010. Behaviour of rare earth elements and yttrium in ferromanganese concretions, gibbsite spots, and the surrounding terra rossa over dolomite during chemical weathering. Chem. Geol. 271, 112–132.

Ferrier, K.L., Kirchner, J.W., Finkel, R.C., 2011. Estimating millennial-scale rates of dust incorporation into eroding hillslope regolith using cosmogenic nuclides and immobile weathering tracers. J. Geophys. Res. 116, F03022. http://dx.doi.org/10.1029/2011JF001991.

Gangloff, S., Stille, P., Pierret, M., Weber, T., Chabaux, F., 2014. Characterization and evolution of dissolved organic matter in acidic forest soil and its impact on the mobility of major and trace elements (case of the Strengbach watershed)Geochim. Cosmochim. Acta 130, 21–41.

Goldberg, E., Smith, R., Koide, M., Schmitt, R., 1963. Rare-earth distributions in marine environment. J. Geophys. Res. 68, 4209–4217.

Goyne, K.W., Brantley, S.L., Chorover, J., 2010. Rare earth element release from phosphate minerals in the presence of organic acids. Chem. Geol. 278, 1–14.

Gruau, G., Dia, A., Olivie-Lauqueta, G., Davranche, M., Pinay, G., 2004. Controls on the distribution of rare earth elements in shallow groundwaters. Water Res. 38, 3576–3586.

Grybos, M., Davranche, M., Gruau, G., Petitjean, P., 2007. Is trace metal release in wetland soils controlled by organic matter mobility or Fe-–oxyhydroxides reduction? J. Colloid Interface Sci. 314, 490–501.

Guo, H., Zhang, B., Wang, G., Shen, Z., 2010. Geochemical controls on arsenic and rare earth elements approximately along a groundwater flow path in the shallow aquifer of the Hetao Basin, Inner Mongolia Chem. Geol. 270, 117–125.

Henderson, P., 1996. In: Jones, A.P. (Ed.), Rare Earth Minerals: Chemistry, Origin and Ore Deposits. Chapman & Hall, pp. 1–17.

Holder, M., Brown, K., Thomas, J., Zabcik, D., Murray, H., 1991. Capillary-wick unsaturated zone soil pore water sampler. Soil Sci. Soc. Am. J. 55, 1195–1202.

Jackson, M.L., 2005. Soil Chemical Analysis: Advanced Course, 2nd ed. Parallel Press, Madison, WI.

Johannesson, K., Stetzenbach, K., Hodge, V., 1997. Rare earth elements as geochemical tracers of regional groundwater mixing. Geochim. Cosmochim. Acta 61, 3605–3618.
Johannesson, K., Tang, J., Daniels, J., Bounds, W., Burdige, D., 2004. Rare earth element concentrations and speciation in organic-rich blackwaters of the Great Dismal Swamp, Virginia. USA Chem. Geol. 209, 271–294.
Johannesson, K.H., Telfeyan, K., Chevis, D.A., Rosenheim, B.E., Leybourne, M.I., 2014. Rare earth elements in stromatolites — 1. Evidence that modern terrestrial stromatolites fractionate rare earth elements during incorporation from ambient waters. In: Dilek, Y., Furnes, H. (Eds.), Evolution of Archean Crust and Early Life. Springer, Dordrecht, pp. 385–411.
Kaplan, D., Bertsch, P., Adriano, D., 1997. Mineralogical and physicochemical differences between mobile and nonmobile colloidal phases in reconstructed pedons. Soil Sci. Soc. Am. J. 61, 641–649.
Laveuf, C., Cornu, S., 2009. A review on the potentiality of rare earth elements to trace pedogenetic processes. Geoderma 154, 1–12.
Laveuf, C., Cornu, S., Juillot, F., 2008. Rare earth elements as tracers of pedogenetic processes. C. R. Geosci. 340, 523–532.
Laveuf, C., Cornu, S., Guilherme, L.R.G., Guerin, A., Juillot, F., 2012. The impact of redox conditions on the rare earth element signature of redoximorphic features in a soil sequence developed from limestone. Geoderma 170, 25–38.
Leybourne, M.I., Johannesson, K.H., 2008. Rare earth elements (REE) and yttrium in stream waters, stream sediments, and Fe-Mn oxyhydroxides: fractionation, speciation, and controls over REE plus Y patterns in the surface environment RID B-2541-2009. Geochim. Cosmochim. Acta 72, 5962–5983.
Livingstone, D.A., 1963. Chemical Composition of Rivers and Lakes. In: Fleischer, M. (Ed.), Data of Geochemistry. U.S. Geol. Survey Prof, p. G1-G64 (paper 440).
London, D., 1992. Phosphorus in S-type magmas — the P2O5 content of feldspars from peraluminous granites, pegmatites, and rhyolites. Am. Mineral. 77, 126–145.
Ma, L., Jin, L., Brantley, S.L., 2011. How mineralogy and slope aspect affect REE release and fractionation during shale weathering in the Susquehanna/Shale Hills Critical Zone Observatory. Chem. Geol. 290, 31–49.
Martin, J.M., Meybeck, M., 1979. Elemental mass-balance of material carried by major world rivers. Mar. Chem. 7, 173–206.
McClain, M., Boyer, E., Dent, C., Gergel, S., Grimm, N., Groffman, P., Hart, S., Harvey, J., Johnston, C., Mayorga, E., McDowell, W., Pinay, G., 2003. Biogeochemical hot spots and hot moments at the interface of terrestrial and aquatic ecosystems. Ecosystems 6, 301–312.
Moffett, J., 1994. A radiotracer study of cerium and manganese uptake onto suspended particles in Chesapeake Bay. Geochim. Cosmochim. Acta 58, 695–703.
Nakajima, T., Terakado, Y., 2003. Rare earth elements in stream waters from the Rokko granite area, Japan: effect of weathering degree of watershed rocks. Geochem. J. 37, 181–198.
Nash, W.P., 1984. Phosphate minerals in terrestrial igneous and metamorphic rocks. In: Nriagu, J.O., Moore, P.B. (Eds.), Phosphate Minerals. Springer, Berlin Heidelberg, pp. 215–241.
NRC, 2001. Basic Research Opportunities in Earth Sciences. National Academies Press, Washington, DC.
Ohta, A., Kawabe, I., 2001. REE(III) adsorption onto Mn dioxide (delta-MnO2) and Fe oxyhydroxide: Ce(III) oxidation by delta-MnO2. Geochim. Cosmochim. Acta 65, 695–703.
Panahi, A., Young, G., Rainbird, R., 2000. Behavior of major and trace elements (including REE) during Paleoproterozoic pedogenesis and diagenetic alteration of an Archean granite near Ville Marie, Quebec, Canada. Geochim. Cosmochim. Acta 64, 2199–2220.
Parshall, R.L., 1950. Measuring Water in Irrigation Channels with Parshall Flumes and Small Weirs, U.S. Soil Conservation Service, Circular No. 843.
Perdrial, J.N., Perdrial, N., Harpold, A., Gao, X., Gabor, R., LaSharr, K., Chorover, J., 2012. Impacts of sampling dissolved organic matter with passive capillary wicks versus aqueous soil extraction. Soil Sci. Soc. Am. J. 76, 2019–2030.
Perdrial, J.N., McIntosh, J., Harpold, A., Brooks, P.D., Zapata-Rios, X., Ray, J., Meixner, T., Kanduc, T., Litvak, M., Troch, P.A., Chorover, J., 2014a. Stream water carbon controls in seasonally snow-covered mountain catchments: impact of inter-annual variability of water fluxes, catchment aspect and seasonal processes. Biogeochemistry 118, 273–290.
Perdrial, J.N., Perdrial, N., Vazquez-Ortega, A., Porter, C., Leedy, J., Chorover, J., 2014b. Experimental assessment of passive capillary wick sampler suitability for inorganic soil solution constituents. Soil Sci. Soc. Am. J. 78, 486–495.
Pokrovsky, O., Schott, J., 2002. Iron colloids/organic matter associated transport of major and trace elements in small boreal rivers and their estuaries (NW Russia). Chem. Geol. 190, 141–179.
Porter, C., 2012. Solute Inputs to Soil and Stream Waters in a Seasonally Snow-covered Mountain Catchment Determined Using Ge/Si, $^{87}SR/^{86}SR$ and Major Ion Chemistry: Valles Caldera(Master Thesis) The University of Arizona, New Mexico (http://hdl.handle.net/10150/265377).
Pourret, O., Martinez, R.E., 2009. Modeling lanthanide series binding sites on humic acid. J. Colloid Interface Sci. 330, 45–50.
Pourret, O., Davranche, M., Gruau, G., Dia, A., 2007a. Organic complexation of rare earth elements in natural waters: evaluating model calculations from ultrafiltration data. Geochim. Cosmochim. Acta 71, 2718–2735.
Pourret, O., Davranche, M., Gruau, G., Dia, A., 2007b. Rare earth elements complexation with humic acid. Chem. Geol. 243, 128–141.
Pourret, O., Gruau, G., Dia, A., Davranche, M., Molenat, J., 2010. Colloidal control on the distribution of rare earth elements in shallow groundwaters. Aquat. Geochem. 16, 31–59.
Reheis, M.C., Budahn, J.R., Lamothe, P.J., 1999. Elemental Analysis of Modern Dust in Southern Nevada and California. USGS OFR 99–531, (http://pubs.usgs.gov/of/1999/ofr-99-0531/).
Ronov, A., Balashov, Y., Migdisov, A., 1967. Geochemistry of rare earths in sedimentary cycle. Geochem. Int. USSR 4, 1–10.
Schnetzl, C.C., Philpott, J.A., 1970. Partition coefficients of rare-earth elements between igneous matrix material and rock-forming mineral phenocrysts.2. Geochim. Cosmochim. Acta 34, 331–340.
Shiller, A.M., 2010. Dissolved rare earth elements in a seasonally snow-covered, alpine/subalpine watershed, Loch Vale, Colorado. Geochim. Cosmochim. Acta 74, 2040–2052.
Sholkovitz, E., 1992. Chemical evolution of rare-earth elements — fractionation between colloidal and ssolution phases of filtered river water. Earth Planet. Sci. Lett. 114, 77–84.
Sonke, J., Salters, V., 2006. Lanthanide-humic substances complexation. I. Experimental evidence for a lanthanide contraction effect. Geochim. Cosmochim. Acta 70, 1495–1506.
Steinmann, M., Stille, P., 2006. Rare earth element transport and fractionation in small streams of a mixed basaltic-granitic catchment basin (Massif Central, France) J. Geochem. Explor. 88, 336–340.
Steinmann, M., Stille, P., 2008. Controls on transport and fractionation of the rare earth elements in stream water of a mixed basaltic-granitic catchment basin (Massif Central, France) Chem. Geol. 254, 118.
Stille, P., Steinmann, M., Pierret, M., Gauthier-Lafaye, F., Chabaux, F., Viville, D., Pourcelot, L., Matera, V., Aouad, G., Aubert, D., 2006. The impact of vegetation on REE fractionation in stream waters of a small forested catchment (the Strengbach case)Geochim. Cosmochim. Acta 70, 3217–3230.
Stille, P., Pierret, M., Steinmann, M., Chabaux, F., Boutin, R., Aubert, D., Pourcelot, L., Morvan, G., 2009. Impact of atmospheric deposition, biogeochemical cycling and water–mineral interaction on REE fractionation in acidic surface soils and soil water (the Strengbach case). Chem. Geol. 264, 173–186.
Susetyo, W., Carreira, L., Azarraga, L., Grimm, D., 1991. Fluorescence techniques for metal–humic interactions. Fresenius J. Anal. Chem. 339, 624–635.
Tang, J., Johannesson, K., 2003. Speciation of rare earth elements in natural terrestrial waters: assessing the role of dissolved organic matter from the modeling approach. Geochim. Cosmochim. Acta 67, 2321–2339.
Tang, J., Johannesson, K.H., 2010a. Ligand extraction of rare earth elements from aquifer sediments: implications for rare earth element complexation with organic matter in natural waters. Geochim. Cosmochim. Acta 74 (6690), 6690–6705.
Tang, J., Johannesson, K.H., 2010b. Rare earth elements adsorption onto Carrizo sand: influence of strong solution complexation. Chem. Geol. 279, 120–133.
Taylor, S., McLennan, S., 1981. The composition and evolution of the continental-crust — rare-earth element evidence from sedimentary-rocks. Philos. Trans. R. Soc. Lond. Ser. A Math. Phys. Eng. Sci. 301, 381–399.
Thompson, A., Chadwick, O.A., Boman, S., Chorover, J., 2006a. Colloid mobilization during soil iron redox oscillations. Environ. Sci. Technol. 40, 5743–5749.
Thompson, A., Chadwick, O.A., Rancourt, D.G., Chorover, J., 2006b. Iron-oxide crystallinity increases during soil redox oscillations. Geochim. Cosmochim. Acta 70, 1710–1727.
Thompson, A., Amistadi, M.K., Chadwick, O.A., Chorover, J., 2013. Fractionation of yttrium and holmium during basaltic soil weathering. Geochim. Cosmochim. Acta 119, 18–30.
Vázquez-Ortega, A., Hernandez-Ruiz, S., Amistadi, M.K., Rasmussen, C., Chorover, J., 2014s. Fractionation of dissolved organic matter by (oxy)hydroxide-coated sands: competitive sorbate displacement during reactive transport. Vadose Zone J. 13, 1–13.
Viers, J., Dupre, B., Polve, M., Schott, J., Dandurand, J., Braun, J., 1997. Chemical weathering in the drainage basin of a tropical watershed (Nsimi-Zoetele site, Cameroon): comparison between organic-poor and organic-rich waters. Chem. Geol. 140, 181–206.
Voegelin, A.R., Naegler, T.F., Pettke, T., Neubert, N., Steinmann, M., Pourret, O., Villa, I.M., 2012. The impact of igneous bedrock weathering on the Mo isotopic composition of stream waters: natural samples and laboratory experiments. Geochim. Cosmochim. Acta 86, 150–165.
Willis, S.S., Johannesson, K.H., 2011. Controls on the geochemistry of rare earth elements in sediments and groundwaters of the Aquia aquifer, Maryland, USA. Chem. Geol. 285, 32–49.
Wood, S.A., 1990. The aqueous geochemistry of the rare-earth elements and yttrium: 1. Review of available low-temperature data for inorganic complexes and the inorganic REE speciation of natural waters. Chem. Geol. 82, 159–186.
Xiong, Y., 2011. Organic species of lanthanum in natural environments: implications to mobility of rare earth elements in low temperature environments. Appl. Geochem. 26, 1130–1137.
Yamamoto, Y., Takahashi, Y., Shimizu, H., 2010. Systematic change in relative stabilities of REE-humic complexes at various metal loading levels. Geochem. J. 44, 39–63.